

# Efficient Variational Inference for Large Skew-t Copulas with Application to Intraday Equity Returns

Lin Deng, Michael Stanley Smith and Worapree Maneesoonthorn

August 11, 2023

Lin Deng is a PhD student and Michael Smith is Professor of Management (Econometrics), both at the Melbourne Business School, University of Melbourne, Australia. Worapree Maneesoonthorn is Associate Professor of Statistics and Econometrics at Monash University, Australia. Correspondence should be directed to Michael Smith at [mikes70au@gmail.com](mailto:mikes70au@gmail.com).

**Acknowledgments:** This research was supported by The University of Melbourne's Research Computing Services and the Petascale Campus Initiative. A/Prof. Maneesoonthorn has been supported by the Australian Research Council (ARC) Discovery Project Grant (DP200101414).

# Efficient Variational Inference for Large Skew-t Copulas with Application to Intraday Equity Returns

## Abstract

Large skew-t factor copula models are attractive for the modeling of financial data because they allow for asymmetric and extreme tail dependence. We show that the copula implicit in the skew-t distribution of Azzalini and Capitanio (2003) allows for a higher level of pairwise asymmetric dependence than two popular alternative skew-t copulas. Estimation of this copula in high dimensions is challenging, and we propose a fast and accurate Bayesian variational inference (VI) approach to do so. The method uses a conditionally Gaussian generative representation of the skew-t distribution to define an augmented posterior that can be approximated accurately. A fast stochastic gradient ascent algorithm is used to solve the variational optimization. The new methodology is used to estimate copula models for intraday returns from 2017 to 2021 on 93 U.S. equities. The copula captures substantial heterogeneity in asymmetric dependence over equity pairs, in addition to the variability in pairwise correlations. We show that intraday predictive densities from the skew-t copula are more accurate than from some other copula models, while portfolio selection strategies based on the estimated pairwise tail dependencies improve performance relative to the benchmark index.

**Keywords:** Asymmetric Dependence, Bayesian Data Augmentation, Factor Copula, Intraday Asset Returns, Variational Bayes.

# 1 Introduction

Copula models are widely employed for multivariate data because they separate the selection of marginals from the copula function. When modeling financial data, the copula should possess two features. First, it should allow for asymmetric dependence, where the level of dependence varies across different quantiles of the variables. Second, it should allow for high tail dependence, where extreme values of both variables are positively or negatively dependent. Skew-t factor copulas can capture both features in high dimensions. However, there exist multiple variants of skew-t copulas, with no consensus on the most effective choice. Moreover, estimation in high dimensions is challenging, particularly for a larger number of factors. This paper addresses both issues by showing that the skew-t factor copula implicit in the Azzalini and Capitanio (2003) distribution, combined with recent advances in Bayesian variational inference, offers an attractive solution. We employ the methodology in a study using 15 minute intraday returns on 93 U.S. equities, and show that pairwise asymmetric dependence varies in a complex fashion over equity pairs and time.

A skew-t copula is that implicit in a parametric skew-t distribution, of which three types have been used previously. The first was proposed by Demarta and Mcneil (2005) and is based on the generalized hyperbolic (GH) skew-t distribution. It is the most popular of the three in financial studies, with applications by Christoffersen et al. (2012), Creal and Tsay (2015), Oh and Patton (2017), Lucas et al. (2017) and Oh and Patton (2023). The second was suggested by Smith et al. (2010) and is based on the distribution of Sahu et al. (2003), while the third proposed by Kollo and Pettere (2010) and Yoshihara (2018) is based on the distribution of Azzalini and Capitanio (2003), which we label the “AC skew-t copula”. All three skew-t distributions have latent conditionally Gaussian generative representations for which factor models can be used, and the resulting implicit copulas are called “factor copulas” by Oh and Patton (2017).<sup>1</sup> In this paper we show the AC skew-t copula allows for higher levels of asymmetry in pairwise dependence than the other two copulas, making it an attractive choice for financial data.

---

<sup>1</sup>This type of factor copula is not to be confused with the similarly named vine-based factor copulas of Krupskii and Joe (2013) and others, which are not the implicit copulas of high-dimensional skew-t distributions studied here.

Yoshihara (2018) carefully studies maximum likelihood estimation of the AC skew-t copula in low dimensions. However, the likelihood (and therefore also posterior) has a complex geometry and its direct optimization is hard in high dimensions, which has precluded its use with large financial panels. Here we propose a scalable solution that uses the conditionally Gaussian generative representation of the skew-t distribution. Latent variables are introduced that can be augmented with the copula parameters to provide a tractable joint (or “augmented”) posterior. However, evaluation of the augmented posterior using Markov chain Monte Carlo (MCMC) methods is too slow to use in high dimensions. To overcome this we develop a new variational inference estimator for evaluating the proposed augmented posterior of the AC skew-t copula in high dimensions.

Variational inference (VI) approximates a target density with a tractable density called a variational approximation (VA). The VA is calibrated by solving an optimization problem where the Kullback-Leibler divergence between it and the target density is minimized. Well designed VI methods are effective for estimating models with large numbers of parameters and/or big datasets; see Blei et al. (2017) for an introduction. But here, the complex geometry of the posterior of the AC skew-t copula parameters means it is difficult to approximate with a simple fixed form density. Therefore, we instead use the augmented posterior of the AC skew-t copula as the target density, and then adopt a VA of the form suggested by Loaiza-Maya et al. (2022). This VA density comprises a Gaussian density with factor covariance matrix (Ong et al., 2018) for the marginal approximation of the copula parameters, along with the exact conditional posterior of the latent variables. To solve the optimization problem stochastic gradient ascent (Bottou, 2010, Ranganath et al., 2014) is used with efficient re-parameterization gradients (Kingma and Welling, 2014). To increase the speed of the method we derive these gradients analytically. The speed and accuracy of the resulting VI method is demonstrated using simulated data.

We use our new copula methodology in two examples using 15 minute intraday financial data. The first illustrates the flexibility of the AC skew-t copula by modeling returns on two equities and the VIX index during two 40 day periods: a low market volatility period, and the high market volatility period of the COVID-19 pandemic crash. There are strong asymmetries in the pairwise

dependencies, which change in direction and scale from the low to high volatility periods.

The second example is our main study, and uses an AC skew-t factor copula to capture dependence between returns on 93 equities. Using a rolling window of width 40 trading days fit from January 2017 to December 2021, we consider three research questions. First, we show that one-step-ahead forecast densities are more accurate than those from benchmark copula models. Interestingly, density forecast accuracy is maximized with 10 to 15 factors, suggesting a rich factor structure is worthwhile. This is consistent with Oh and Patton (2017), Opschoor et al. (2021) and Oh and Patton (2023), who find that industry or other group-based factors improve performance. Second, a major finding of this paper is that pairwise dependence asymmetries can differ substantially over equity pairs. Most previous studies focus on the heterogeneity in cross-sectional correlation, and our results suggest dependence asymmetry also exhibits a high level of heterogeneity. Last, we show that (absent of trading costs) portfolio selection strategies based on pairwise tail dependencies from the copula model can improve performance relative to index returns.

Skew-t factor copulas have been used previously to capture dependence in high dimensional financial data. Oh and Patton (2013) use the implicit copula of the GH distribution, and of a mixture of GH and t distributions. Creal and Tsay (2015) and Oh and Patton (2023) consider the implicit copula of the GH distribution with a global factor, which Oh and Patton (2023) augments with latent group specific factors. Lucas et al. (2017) considers the same copula with a block equicorrelation structure. In comparison, ours is the first paper of which we are aware to use the AC skew-t copula for a large financial panel. We adopt an unrestricted specification for the skew parameters of the skew-t distribution, allowing for high levels of heterogeneity in pairwise tail dependence in its implicit copula. Previous studies consider dynamic latent factor specifications for fitting daily or weekly financial time series. In contrast, we employ intraday data at the 15 minute frequency in a rolling window study using a static factor model with up to 15 global factors. Our objective is to allow for a high degree of heterogeneity in the level of asymmetric dependence over equity pairs, rather than capturing time variation at a lower data frequency.

Our paper also contributes to the literature on Bayesian estimation of skew-t copulas. Creal

and Tsay (2015) use MCMC to estimate their skew-t factor copula, where a particle filter is used to evaluate the intractable likelihood. Smith et al. (2010) use MCMC with data augmentation, but for the skew-t copula implicit in the distribution of Sahu et al. (2003). Both approaches can also be adopted to estimate the AC skew-t copula, but they incur a much higher computational burden than the VI approach suggested here. A few recent studies have used VI methods to estimate other high-dimensional copula models. Loaiza-Maya and Smith (2019) use VI to estimate vine copulas with discrete margins, while Nguyen et al. (2020) use VI to estimate factor copulas based on pair-copula constructions suggested by Krupskii and Joe (2013). However, both studies employ simple mean field or other fixed form VAs that are ineffective approximations for the complex geometry of the posterior of the skew-t copula. In contrast, the augmented posterior that we employ has a simpler geometry that can be approximated accurately using the VA we propose.

The rest of the paper is organized as follows. Section 2 outlines the three skew-t copulas. Section 3 develops the variational inference method for estimating the AC skew-t factor copula, and its efficacy is demonstrated using simulated data in Section 4. Section 5 contains the two empirical studies of intraday equity returns, while Section 6 concludes.

## 2 Skew-t Copulas

### 2.1 Copula models

A copula model (Nelsen, 1999, Joe, 2014) expresses the joint distribution function of a continuous-valued random vector  $\mathbf{Y} = (Y_1, \dots, Y_d)^\top$  as

$$F_Y(\mathbf{y}) = C(F_{Y_1}(y_1), \dots, F_{Y_d}(y_d)). \quad (1)$$

Here,  $\mathbf{y} = (y_1, \dots, y_d)^\top$ ,  $F_{Y_j}$  is the marginal distribution function of  $Y_j$ , and  $C : [0, 1]^d \rightarrow \mathbb{R}$  is a copula function that captures the dependence structure. Differentiating (1) gives the joint density

$$f_Y(\mathbf{y}) = \frac{\partial}{\partial \mathbf{y}} F_Y(\mathbf{y}) = c(F_{Y_1}(y_1), \dots, F_{Y_d}(y_d)) \prod_{j=1}^d f_{Y_j}(y_j), \quad (2)$$

where  $f_{Y_j} = \frac{\partial}{\partial y_j} F_{Y_j}(y_j)$ ,  $c(\mathbf{u}) = \frac{\partial}{\partial \mathbf{u}} C(\mathbf{u})$  is widely called the ‘‘copula density’’, and  $\mathbf{u} = (u_1, \dots, u_d)^\top$ .<sup>2</sup>

The main advantage of using a copula model is that the marginals and the copula function can be modeled separately. When the elements of  $\mathbf{Y}$  are asset returns, their distribution features asymmetric and high tail dependence; e.g. see Patton (2006) and Christoffersen et al. (2012). A skew-t copula is one of only a few copulas that can account for these features in high dimensions.

## 2.2 Three skew-t copulas

Let the continuous random vector  $\mathbf{Z} = (Z_1, \dots, Z_d)^\top \sim F_Z$ , with marginals  $F_{Z_1}, \dots, F_{Z_d}$ . Then if  $U_j = F_{Z_j}(Z_j)$ , the distribution function of  $\mathbf{U} = (U_1, \dots, U_d)^\top$  is  $C(\mathbf{u}) = F_Z(F_{Z_1}^{-1}(u_1), \dots, F_{Z_d}^{-1}(u_d))$ . This is called an implicit copula, and the elements of  $\mathbf{Z}$  are called pseudo or auxiliary variables because their values are unobserved; see Smith (2021) for an introduction. The copula density is

$$c(\mathbf{u}) = \frac{\partial}{\partial \mathbf{u}} C(\mathbf{u}) = f_Z(\mathbf{z}) / \prod_{j=1}^d f_{Z_j}(z_j), \quad (3)$$

where  $\mathbf{z} = (z_1, \dots, z_d)^\top$ ,  $f_Z(\mathbf{z}) = \frac{\partial}{\partial \mathbf{z}} F_Z(\mathbf{z})$  and  $f_{Z_j} = \frac{\partial}{\partial z_j} F_{Z_j}(z_j)$ . A skew-t copula is where  $F_Z$  is a multivariate skew-t distribution. Because there are different skew-t distributions (e.g. see Genton (2004)), there are also different copulas. Three types have been used previously, which we briefly outline below. The marginal moments of  $\mathbf{Z}$  are unidentified in  $C$ , so that location parameters are unnecessary and the scale matrices are restricted to be a correlation matrix  $\bar{\Omega}$ .

### 2.2.1 GH skew-t copula

Demarta and Mcneil (2005) construct the implicit copula of the generalized hyperbolic (GH) skew-t distribution (Barndorff-Nielsen, 1977). This distribution has the generative representation

$$\mathbf{Z}_{\text{GH}} = \boldsymbol{\delta} W + W^{-1/2} \mathbf{X},$$

where  $\mathbf{X} \sim N_d(\mathbf{0}, \bar{\Omega})$ ,  $W \sim \text{Gamma}(\nu/2, \nu/2)$ , and  $\boldsymbol{\delta} \in \mathbb{R}^d$  is the skewness parameter. The joint density of  $\mathbf{Z}_{\text{GH}}$  is available in closed form (see Part A of the Web Appendix). However, the marginal distribution and quantile functions are not and are difficult to compute using numerical methods,

<sup>2</sup>The notation  $C(u_1, \dots, u_d)$  and  $C(\mathbf{u})$  are considered equivalent, as is the notation  $c(u_1, \dots, u_d)$  and  $c(\mathbf{u})$ .

so that they are usually evaluated by Monte Carlo simulation from the generative representation. When  $d$  is high this can be slow, although setting  $\boldsymbol{\delta} = \delta(1, 1, \dots, 1)^\top$  with  $\delta$  a scalar (Oh and Patton, 2023) speeds computation greatly, but at the cost of restricting the flexibility of the pairwise asymmetric dependencies in its implicit copula.

### 2.2.2 SDB skew-t copula

Smith et al. (2010) construct the implicit copula of the skew-t distribution proposed by Sahu et al. (2003). This distribution can be constructed from a t-distribution by hidden conditioning as follows.

Let  $\mathbf{X}$  and  $\mathbf{L}$  be  $d$ -dimensional random variables jointly distributed

$$\begin{pmatrix} \mathbf{X} \\ \mathbf{L} \end{pmatrix} \sim t_{2d}(\mathbf{0}, \Omega, \nu), \Omega = \begin{pmatrix} \bar{\Omega} + D^2 & D \\ D & I \end{pmatrix},$$

with  $D = \text{diag}(\boldsymbol{\delta})$ ,  $\boldsymbol{\delta} \in \mathbb{R}^d$ ,  $\bar{\Omega}$  a positive definite matrix, and  $t_{2d}(\mathbf{0}, \Omega, \nu)$  denoting a t-distribution with mean zero, scale matrix  $\Omega$  and  $\nu$  degrees of freedom. Then,  $\mathbf{Z}_{\text{SDB}} \equiv (\mathbf{X} | \mathbf{L} > \mathbf{0})$ <sup>3</sup> is a skew-t distribution with skewness parameters  $\boldsymbol{\delta}$  and joint density  $f_{\mathbf{Z}_{\text{SDB}}}(\mathbf{z}; \bar{\Omega}, \boldsymbol{\delta}, \nu) = 2^d f_t(\mathbf{z}; \mathbf{0}, \bar{\Omega} + D^2, \nu) \Pr(\mathbf{V} > \mathbf{0}; \mathbf{z})$  where  $f_t(\mathbf{z}; \mathbf{0}, \bar{\Omega}, \nu)$  is the density of a  $t_d(\mathbf{0}, \bar{\Omega}, \nu)$  distribution evaluated at  $\mathbf{z}$ , and  $\mathbf{V}$  follows a  $d$ -dimensional t-distribution with parameters that are functions of  $\mathbf{z}$ . Sahu et al. (2003) show that the  $j$ th marginal has density  $f_{\mathbf{Z}_{\text{SDB}}}(z_j; 1, \delta_j, \nu)$  with distribution and quantile functions that are computed numerically. Evaluation of the copula density at (3) for large  $d$  is difficult because computation of the term  $\Pr(\mathbf{V} > \mathbf{0}; \mathbf{z})$  is also. However, Smith et al. (2010) show how to estimate the distribution and its implicit copula using Bayesian data augmentation.

### 2.2.3 AC skew-t copula

Kollo and Pettere (2010) and Yoshida (2018) construct the implicit copula of the skew-t distribution proposed by Azzalini and Capitanio (2003). This distribution is formed via hidden conditioning as

---

<sup>3</sup>The notation  $\mathbf{X} | \mathbf{L} > \mathbf{0}$  corresponds to the conditional distribution of  $\mathbf{X}$  given that all elements of  $\mathbf{L}$  are positive. It does not denote the conditional distribution of  $\mathbf{X}$  given a specific value for  $\mathbf{L}$ . This notational convention is used throughout the paper.



follows. Let  $\mathbf{X}$  be a  $d$ -dimensional random vector and  $L$  a random variable with joint distribution

$$\begin{pmatrix} \mathbf{X} \\ L \end{pmatrix} \sim t_{d+1}(\mathbf{0}, \Omega, \nu), \quad \Omega = \begin{pmatrix} \bar{\Omega} & \boldsymbol{\delta} \\ \boldsymbol{\delta}^\top & 1 \end{pmatrix}, \quad (4)$$

where  $\boldsymbol{\delta} = (\delta_1, \dots, \delta_d)^\top$ . Then,  $\mathbf{Z}_{\text{AC}} \equiv (\mathbf{X}|L > 0)$  is a skew- $t$  distribution with joint density

$$f_{\mathbf{Z}_{\text{AC}}}(\mathbf{z}; \bar{\Omega}, \boldsymbol{\delta}, \nu) = 2f_t(\mathbf{z}; \mathbf{0}, \bar{\Omega}, \nu)T\left(\boldsymbol{\alpha}^\top \mathbf{z} \sqrt{\frac{\nu + d}{\nu + \mathcal{M}(\mathbf{z})}}; \nu + d\right), \quad (5)$$

where  $\mathcal{M}(\mathbf{z}) = \mathbf{z}^\top \bar{\Omega}^{-1} \mathbf{z}$ , and  $T(x; \nu)$  is the distribution function of a univariate student- $t$  with degrees of freedom  $\nu$ , evaluated at  $x$ . There is a one-to-one relationship between  $\boldsymbol{\alpha}$  and  $\boldsymbol{\delta}$ , given by

$$\boldsymbol{\alpha} = (1 - \boldsymbol{\delta}^\top \bar{\Omega}^{-1} \boldsymbol{\delta})^{-1/2} \bar{\Omega}^{-1} \boldsymbol{\delta}, \quad \text{and} \quad \boldsymbol{\delta} = (1 + \boldsymbol{\alpha}^\top \bar{\Omega} \boldsymbol{\alpha})^{-1/2} \bar{\Omega} \boldsymbol{\alpha}.$$

It is often more convenient to employ  $\boldsymbol{\alpha} \in \mathbb{R}^d$  as the skewness parameter, rather than  $\boldsymbol{\delta}$ , because it is unconstrained. The  $j$ th marginal of (5) has density  $f_{\mathbf{Z}_{\text{AC}}}(z_j; \delta_j, \nu)$ , and the distribution function  $F_j(z_j; \delta_j, \nu) = \int_{-\infty}^{z_j} f_{\mathbf{Z}_{\text{AC}}}(\xi; \delta_j, \nu) d\xi$  is computed using numerical integration.

A draw from the AC skew- $t$  distribution can be obtained by first generating  $W \sim \text{Gamma}(\nu/2, \nu/2)$ , followed by  $\tilde{L} \sim N(0, 1)$  constrained so that  $\tilde{L} > 0$ , and then

$$\mathbf{Z}_{\text{AC}} | \tilde{L}, W \sim N_d\left(\frac{\tilde{L}}{\sqrt{W}} \boldsymbol{\delta}, \frac{1}{W} (\bar{\Omega} - \boldsymbol{\delta} \boldsymbol{\delta}^\top)\right), \quad (6)$$

where  $\tilde{L} = W^{1/2}L$ , with  $L$  defined at (4). Two alternative generative representations for the AC skew- $t$  distribution are given in Appendix B. To convert a draw  $\mathbf{Z}_{\text{AC}} = (Z_1, \dots, Z_d)^\top$  from the skew- $t$  distribution to a draw  $\mathbf{U} \sim C$  from its implicit copula, set  $U_j = F_j(Z_j; \delta_j, \nu)$  for all  $j$ .

### 2.3 Asymmetric dependence

The main motivation for using a skew- $t$  copula is to capture asymmetric dependence in high dimensions. To measure this here we compute the four pairwise quantile dependence metrics, and define measures of asymmetry in the major and minor diagonals as follows. Let  $(Y_1, Y_2)$  follow a bivariate copula model<sup>4</sup> with copula function  $C(u_1, u_2) = \Pr(U_1 \leq u_1, U_2 \leq u_2)$ . Then, for  $0 < u < 0.5$ ,

<sup>4</sup>Because all three skew- $t$  distributions are closed under marginalization, so are the skew- $t$  copulas. Therefore, maximum asymmetric tail dependence in the bivariate case is equal to that for variable pairs in higher dimensions.

we define the four quantile dependencies as: lower left  $\lambda_{LL}(u) = P(U_2 \leq u|U_1 \leq u)$ , upper right  $\lambda_{UR}(u) = P(U_2 > 1 - u|U_1 > 1 - u)$ , lower right  $\lambda_{LR}(u) = P(U_2 \leq u|U_1 > 1 - u)$ , and upper left  $\lambda_{UL}(u) = P(U_2 > 1 - u|U_1 \leq u)$ . They are computed for the AC and SDB skew-t copulas using numerical integration, and by Monte Carlo simulation for the GH skew-t copula; see Appendix A for more details. For a given value  $u$ , the metrics

$$\Delta_{\text{Major}}(u) \equiv \lambda_{UR}(u) - \lambda_{LL}(u), \text{ and } \Delta_{\text{Minor}}(u) \equiv \lambda_{UL}(u) - \lambda_{LR}(u),$$

measure asymmetry in the major and minor diagonals, respectively.

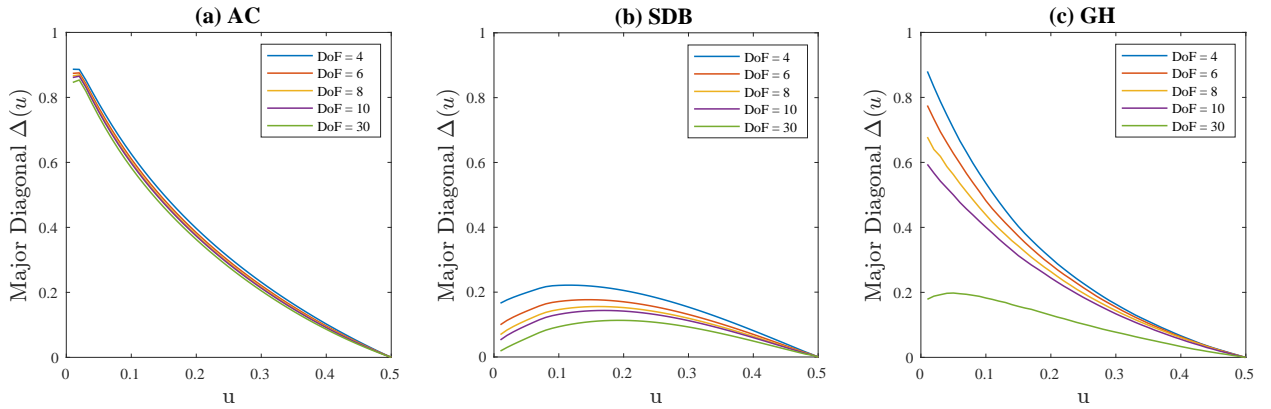


Figure 1: Maximum asymmetric dependence  $\Delta(u)$  of the three skew-t copulas (a) AC, (b) SDB, and (c) GH. Results are given for degrees of freedom  $\nu = 4, 6, 8, 10, 30$ , and plotted as a function of  $u$ .

The maximum asymmetry for each of the three copulas is obtained by solving the optimization

$$\max_{\delta, \rho} \{\Delta(u)\}$$

for given values of  $0 < u < 0.5$  and  $\nu$ . The solution is the same for  $\Delta_{\text{Major}}(u)$  and  $\Delta_{\text{Minor}}(u)$ , and optimization is with respect to  $\delta = (\delta_1, \delta_2)$  and the off-diagonal element  $\rho$  of the  $(2 \times 2)$  correlation matrix  $\bar{\Omega}$ . Figure 1 plots the maximums against  $u$ . At every quantile the GH skew-t copula has a higher maximum asymmetric dependence than the SDB skew-t copula. However, the AC skew-t copula has a higher maximum level of asymmetric dependence than both alternatives for all but the lowest values of  $\nu$ , at which  $\Delta(u)$  is almost equal for the AC and GH skew-t copulas. Figure A1 in the Web Appendix plots contours of the bivariate densities for the three copulas with maximal

$\Delta_{\text{Major}}(0.01)$ , further illustrating the strong differences between the skew-t copulas

In summary, the choice of skew-t copula allows for different levels of maximal asymmetric dependence. In this regard, the AC copula is an attractive choice, and we employ it here.

## 2.4 Factor copula

For large  $d$  an unrestricted correlation matrix  $\bar{\Omega}$  is difficult estimate, and one solution is adopt a factor model for the auxiliary variables  $\mathbf{Z}$ . Following Murray et al. (2013), a static factor copula is used here, which corresponds to adopting the factorization

$$\bar{\Omega} = V_1 V V_1 = V_1 (G G^\top + D) V_1. \quad (7)$$

Here,  $G = \{g_{ij}\}$  is an  $(d \times k)$  loadings matrix with  $k \ll d$ , zero upper triangle and positive leading diagonal elements (i.e.  $g_{ii} > 0$ ), and to identify the parameters  $D = I_d$ . The diagonal matrix  $V_1 = \text{diag}(V)^{-1/2}$  normalizes  $V$  to a correlation matrix. If  $\tilde{G}$  equals  $G$  with the leading diagonal elements replaced by their logarithmic values, then  $\bar{\Omega}$  is parameterized by  $\text{vech}(\tilde{G})$ .

## 3 Variational Inference for the AC Copula

### 3.1 Likelihood

Consider observations  $\mathbf{y}_i = (y_{i1}, \dots, y_{id})^\top$ , for  $i = 1, \dots, n$ , drawn independently from the copula model at (1) with copula parameters  $\boldsymbol{\theta}$ . The pseudo variables  $\mathbf{z}_i = (z_{i1}, \dots, z_{id})^\top$  are given by

$$z_{ij} = F_{Z_j}^{-1}(F_{Y_j}(y_{ij}); \boldsymbol{\theta}), \quad (8)$$

where  $F_{Z_j}$  is a function of  $\boldsymbol{\theta}$ . If  $\mathbf{y} = \{\mathbf{y}_1, \dots, \mathbf{y}_n\}$ , then from (2) and (3), the likelihood is

$$p(\mathbf{y}|\boldsymbol{\theta}) = \prod_{i=1}^n \left\{ p(\mathbf{z}_i|\boldsymbol{\theta}) \prod_{j=1}^d \frac{f_{Y_j}(y_{ij})}{f_{Z_j}(z_{ij}; \boldsymbol{\theta})} \right\}.$$

For the AC skew-t copula, plots of the likelihood (unreported) show that it has a complex geometry, making direct maximization challenging for large  $d$ . However, more tractable extended likelihoods of the copula model can be obtained from generative representations of the skew-t distributions of

**Z.** These can be used with Bayesian data augmentation methods as we now outline.

### 3.2 Extended likelihood for the AC Copula Model

An extended likelihood can be defined using the generative representation for the AC skew-t distribution given in Section 2.2.3. Let  $\mathbf{w} = (w_1, \dots, w_n)^\top$  be a vector  $n$  draws of  $W$ , and  $\tilde{\mathbf{l}} = (\tilde{l}_1, \dots, \tilde{l}_n)^\top$  be a vector of  $n$  draws of  $\tilde{L}$ , then

$$p(\mathbf{y}, \tilde{\mathbf{l}}, \mathbf{w} | \boldsymbol{\theta}) = \prod_{i=1}^n p(\mathbf{y}_i, \tilde{l}_i, w_i | \boldsymbol{\theta}) = \prod_{i=1}^n \left\{ p(\mathbf{z}_i, \tilde{l}_i, w_i | \boldsymbol{\theta}) \prod_{j=1}^d \frac{f_{Y_j}(y_{ij})}{f_{Z_j}(z_{ij})} \right\}, \quad (9)$$

is the extended likelihood. The product over  $j$  in (9) is the Jacobian of the transformation from  $\mathbf{z}$  to  $\mathbf{y}$  at (8). From the generative representation of the AC skew-t distribution, the joint density

$$p(\mathbf{z}_i, \tilde{l}_i, w_i | \boldsymbol{\theta}) = p(\mathbf{z}_i | \tilde{l}_i, w_i, \boldsymbol{\theta}) p(\tilde{l}_i | w_i) p(w_i | \nu), \quad (10)$$

where  $p(w_i | \nu)$  is the density of a  $\text{Gamma}(\nu/2, \nu/2)$  distribution,  $p(\tilde{l}_i | w_i) = 2\phi_1(\tilde{l}_i; 0, 1)\mathbf{1}(l_i > 0)$  is the density of a constrained standard normal, and  $p(\mathbf{z}_i | \tilde{l}_i, w_i, \boldsymbol{\theta}) = \phi_d(\mathbf{z}_i; \boldsymbol{\delta} \tilde{l}_i w_i^{-1/2}, w_i^{-1}(\bar{\boldsymbol{\Omega}} - \boldsymbol{\delta} \boldsymbol{\delta}^\top))$ . Here,  $\phi_m(\cdot; \boldsymbol{\mu}, \Sigma)$  denotes the density of a  $N_m(\boldsymbol{\mu}, \Sigma)$  distribution, and the indicator function  $\mathbf{1}(X) = 1$  if  $X$  is true, and zero otherwise. The copula model likelihood can be recovered by integrating over the two latent vectors; i.e.  $p(\mathbf{y} | \boldsymbol{\theta}) = \int p(\mathbf{y}, \tilde{\mathbf{l}}, \mathbf{w} | \boldsymbol{\theta}) d(\tilde{\mathbf{l}}, \mathbf{w})$ .

The advantage of this extended likelihood is that it is tractable and fast to compute. Evaluation of  $F_{Z_1}^{-1}, \dots, F_{Z_d}^{-1}$  is undertaken using the spline interpolation method outlined by Smith and Maneesoonthorn (2018) and Yoshihara (2018) that uses the closed form densities  $f_{Z_1}, \dots, f_{Z_d}$ . These authors show this approach is highly accurate and is scalable with respect to  $n$ . Alternative extended likelihoods can be specified using the other generative representations given in Appendix B, although we found these to be less effective than that adopted here.

### 3.3 Priors and Posterior

The copula parameters with a factor decomposition for  $\bar{\boldsymbol{\Omega}}$  are  $\boldsymbol{\theta} = \{\text{vech}(\tilde{G}), \boldsymbol{\alpha}, \nu\}$ , where  $\boldsymbol{\alpha} = (\alpha_1, \dots, \alpha_d)^\top$  is a one-to-one function of  $\boldsymbol{\delta}$ . Bayesian estimation uses the posterior density  $p(\boldsymbol{\theta} | \mathbf{y})$ ,

which is the marginal in  $\boldsymbol{\theta}$  of the augmented posterior

$$p(\boldsymbol{\theta}, \tilde{\mathbf{l}}, \mathbf{w}|\mathbf{y}) \propto p(\mathbf{y}, \tilde{\mathbf{l}}, \mathbf{w}|\boldsymbol{\theta})p(\boldsymbol{\theta}) \equiv h(\boldsymbol{\psi}), \quad (11)$$

where  $\boldsymbol{\psi} \equiv \{\boldsymbol{\theta}, \tilde{\mathbf{l}}, \mathbf{w}\}$ . The augmented posterior is the product of the extended likelihood at (9) and the prior  $p(\boldsymbol{\theta}) = p(\text{vech}(\tilde{G}))p(\boldsymbol{\alpha})p(\nu)$ . We adopt the generalized double Pareto distribution prior for each element of  $\text{vech}(\tilde{G})$  suggested by Murray et al. (2013). The prior  $\alpha_j \sim N(0, 5^2)$ , which places 99% mass on  $\delta_j \in (-0.997, 0.997)$ . The prior for  $\nu$  is constrained so that  $\nu > 2$ , with  $(\nu - 2) \sim \text{Gamma}(3, 0.2)$ . This places 99% mass on the range  $\nu \in (3.69, 48.47)$ .

An MCMC scheme that produces draws from the augmented posterior of the AC skew-t copula is outlined in Appendix C. However, in high dimensions  $d$  it is slow and variational inference provides a faster and more scalable alternative, as we now discuss.

### 3.4 Hybrid variational inference

VI approximates the augmented posterior using a density  $q(\boldsymbol{\psi}) \in \mathcal{Q}$  called the “variational approximation” (VA) from a family of tractable approximations  $\mathcal{Q}$ . Typically, the VA is obtained by minimizing the Kullback-Leibler divergence (KLD) between the target density  $p(\boldsymbol{\psi}|\mathbf{y}) \propto p(\mathbf{y}|\boldsymbol{\psi})p(\boldsymbol{\psi}) = h(\boldsymbol{\psi})$  and its approximation  $q(\boldsymbol{\psi})$ . It is easily shown that this is equivalent to maximizing the Evidence Lower Bound (ELBO)

$$\mathcal{L} = E_q [\log h(\boldsymbol{\psi}) - \log q(\boldsymbol{\psi})]$$

over  $q \in \mathcal{Q}$ , where the expectation is with respect to  $\boldsymbol{\psi} \sim q$ .

The selection of family  $\mathcal{Q}$  that balances accuracy of the VA and the time required to maximize the ELBO function, is the topic of much current research. For models with a large number of latent variables, such as the augmented posterior at (11), Loaiza-Maya et al. (2022) point out that assuming simple fixed form approximations (such as the widely used mean field approximation) can be very inaccurate. Instead, they suggest using a VA family of the form

$$q_\lambda(\boldsymbol{\psi}) = p(\tilde{\mathbf{l}}, \mathbf{w}|\boldsymbol{\theta}, \mathbf{y})q_\lambda^0(\boldsymbol{\theta}), \quad (12)$$

where  $p(\tilde{\mathbf{l}}, \mathbf{w}|\boldsymbol{\theta}, \mathbf{y})$  is the conditional posterior of the latent variables, and  $q_\lambda^0(\boldsymbol{\theta})$  is the density of a fixed form VA with parameters  $\boldsymbol{\lambda}$  which we discuss further below.<sup>5</sup> These authors show that when using the VA at (12), the ELBO of the target density  $p(\boldsymbol{\psi}|\mathbf{y})$  is exactly equal to the ELBO of the target density  $p(\boldsymbol{\theta}|\mathbf{y})$ ; that is,

$$\mathcal{L} = E_{q_\lambda} [\log h(\boldsymbol{\psi}) - \log q_\lambda(\boldsymbol{\psi})] = E_{q^0} [\log (p(\mathbf{y}|\boldsymbol{\theta})p(\boldsymbol{\theta})) - \log q_\lambda^0(\boldsymbol{\theta})] .$$

Thus, maximizing  $\mathcal{L}$  is equivalent to solving the variational optimization for the parameter posterior with the latent variables  $\{\tilde{\mathbf{l}}, \mathbf{w}\}$  integrated out exactly, which makes (12) more accurate than other choices of VA for this target density.

To maximize  $\mathcal{L}$  with respect to the variational parameters  $\boldsymbol{\lambda}$ , stochastic gradient ascent (SGA) is the most frequently used algorithm (Bottou, 2010, Ranganath et al., 2014). From an initial value  $\boldsymbol{\lambda}^{(0)}$ , SGA recursively updates

$$\boldsymbol{\lambda}^{(t+1)} = \boldsymbol{\lambda}^{(t)} + \boldsymbol{\rho}^{(t)} \circ \widehat{\nabla_\lambda \mathcal{L}} \Big|_{\boldsymbol{\lambda}=\boldsymbol{\lambda}^{(t)}}, \quad t = 0, 1, \dots \quad (13)$$

until reaching convergence. Here,  $\boldsymbol{\rho}^{(t)}$  is a vector of adaptive learning rates set using the momentum method of Zeiler (2012), ‘ $\circ$ ’ is the Hadamard product, and  $\widehat{\nabla_\lambda \mathcal{L}}$  is an unbiased estimator of the gradient, which is evaluated at  $\boldsymbol{\lambda} = \boldsymbol{\lambda}^{(t)}$ . The key to fast convergence and computational efficiency of this SGA algorithm is that  $\widehat{\nabla_\lambda \mathcal{L}}$  has low variability and is fast to evaluate. One of the most effective ways to achieve this is to use the re-parameterization trick of Kingma and Welling (2014). For the VA at (12), the re-parameterization is a transformation from  $\boldsymbol{\theta}$  to  $\boldsymbol{\varepsilon} \sim f_\varepsilon$ , where  $\boldsymbol{\theta} = \tau(\boldsymbol{\varepsilon}, \boldsymbol{\lambda})$  and  $\tau$  is a deterministic function. In this case, it is possible to show that

$$\nabla_\lambda \mathcal{L} = E_{f_{\varepsilon, \tilde{\mathbf{l}}, \mathbf{w}}} \left[ \frac{\partial \boldsymbol{\theta}^\top}{\partial \boldsymbol{\lambda}} (\nabla_\theta \log h(\boldsymbol{\psi}) - \nabla_\theta \log q_\lambda^0(\boldsymbol{\theta})) \right], \quad (14)$$

where the expectation is with respect to the density  $f_{\varepsilon, \tilde{\mathbf{l}}, \mathbf{w}}(\boldsymbol{\varepsilon}, \tilde{\mathbf{l}}, \mathbf{w}) = f_\varepsilon(\boldsymbol{\varepsilon})p(\tilde{\mathbf{l}}, \mathbf{w}|\boldsymbol{\theta}, \mathbf{y})$ .<sup>6</sup> Typically only a single draw from  $f_{\varepsilon, \tilde{\mathbf{l}}, \mathbf{w}}$  is required to obtain a low variance estimate of the expectation in (14),

<sup>5</sup>In the machine learning literature a parametric density  $q_\lambda$  with parameters  $\boldsymbol{\lambda}$  is often called a fixed form density.

<sup>6</sup>In expressing this gradient we adopt the following notation. If  $f(\mathbf{x})$  is a scalar-valued function of a column vector  $\mathbf{x}$ , then  $\nabla_x g(\mathbf{x}) = \frac{\partial g}{\partial \mathbf{x}}^\top$  which is a column vector. If the vector-valued function  $g(\mathbf{x}) \in \mathbb{R}^d \times 1$  and  $\mathbf{x} \in \mathbb{R}^n \times 1$ , then  $\frac{\partial g}{\partial \mathbf{x}}$  is a  $d \times n$  matrix with  $(i, j)$  element  $\frac{\partial g_i}{\partial x_j}$ .

resulting in a major computational advantage.

For  $q_\lambda^0$  we use a Gaussian density with a factor model covariance matrix as suggested by Miller et al. (2017), Ong et al. (2018) and Mishkin et al. (2018) with  $r$  factors. This is not to be confused with the factor model used to define the copula. Ong et al. (2018) give the transformation  $\tau$  required for the re-parametrization trick, fast to compute closed form expressions for the derivatives  $\frac{\partial \theta^\top}{\partial \lambda}$  and  $\nabla_\theta \log q_\lambda^0(\theta)$  in (14), along with MATLAB routines for their evaluation. The derivative

$$\nabla_\theta \log h(\boldsymbol{\psi}) = (\nabla_{\text{vech}(\tilde{G})}^\top \log h(\boldsymbol{\psi}), \nabla_\alpha^\top \log h(\boldsymbol{\psi}), \nabla_\nu^\top \log h(\boldsymbol{\psi}))^\top,$$

is specific to the target density  $p(\boldsymbol{\psi}|\mathbf{y})$ , which is the augmented posterior. Table 1 provides this gradient, which is evaluated recursively from the bottom of the columns upwards. Its derivation is given in Part A of the Web Appendix, and uses the trace operator to express the gradient in a computationally efficient directional derivative form; e.g. see Dattorro (2005, p.439).

Loaiza-Maya et al. (2022) calls an approach that combines the VA at (12) with stochastic gradient ascent optimization and re-parameterized gradients, a “hybrid VI” method. This is because it nests an MCMC step within a well-defined stochastic optimization algorithm for solving the VI problem. Algorithm 1 details our proposed hybrid VI algorithm for estimating the AC skew-t copula. At Step (b) a small number of Gibbs steps that first draw from  $\tilde{\mathbf{l}}|\mathbf{w}, \boldsymbol{\theta}, \mathbf{y}$ , and then from  $\mathbf{w}|\tilde{\mathbf{l}}, \boldsymbol{\theta}, \mathbf{y}$ , are used as outlined in Appendix C. We demonstrate that this works well here, although other methods, such as the Hamiltonian Monte Carlo sampler of Hoffman et al. (2014), can also be used at this step. The output of the algorithm  $q_\lambda^0(\theta)$  is typically called the “variational posterior”, because it is the optimal VA to the parameter posterior  $p(\boldsymbol{\theta}|\mathbf{y})$ .

## 4 Simulation

### 4.1 Design

The efficacy of the VI method is first demonstrated using simulated data from lower dimensional examples where the exact posterior can be calculated. A sample of size  $n = 1024$  is generated

Table 1: Closed form expression for the gradient  $\nabla_{\theta} \log p(\boldsymbol{\theta}, \tilde{\mathbf{l}}, \mathbf{w}|\mathbf{y})$ 

Computing $\nabla_G \log p(\boldsymbol{\theta}, \tilde{\mathbf{l}}, \mathbf{w} \mathbf{y})$	Computing $\nabla_{\alpha} \log p(\boldsymbol{\theta}, \tilde{\mathbf{l}}, \mathbf{w} \mathbf{y})$
$\nabla_G \log p(\boldsymbol{\theta}, \tilde{\mathbf{l}}, \mathbf{w} \mathbf{y})$ $= \nabla_G \left\{ -\frac{n}{2} T_{G1} - \frac{1}{2} \sum_{i=1}^n (T_{G2i} + T_{G3i} + T_{G4i}) \right\}$ $+ \nabla_G \log p(G)$ $\nabla_G T_{G1} = -2(V_2 \odot V V_1 C_4 + V_1 C_4 V_1) G$ $\nabla_G T_{G2i} = -2(V_2 \odot V V_1 C_{7i} + V_1 C_{7i} V_1) G$ $\nabla_G T_{G3i} = -2(V_2 \odot V V_1 C_{11i} + V_1 C_{11i} V_1) G$ $\nabla_G T_{G4i} = -2(V_2 \odot V V_1 C_{15i} + V_1 C_{15i} V_1) G$ $\nabla_G \log p(G) = -(a_1 + 1) \text{sign}(G) \frac{1}{b_1 +  G }$ $C_0 = \bar{\Omega}^{-1} + \frac{\bar{\Omega}^{-1} \boldsymbol{\delta} \boldsymbol{\delta}^{\top} \bar{\Omega}^{-1}}{1 - \boldsymbol{\delta}^{\top} \bar{\Omega}^{-1} \boldsymbol{\delta}}$ $C_1 = 1 + \boldsymbol{\alpha}^{\top} \bar{\Omega} \boldsymbol{\alpha}$ $C_2 = \boldsymbol{\alpha} \boldsymbol{\alpha}^{\top} \bar{\Omega}$ $C_3 = C_1^{-1} C_2 C_0 + C_1^{-1} C_0 C_2^{\top} - C_1^{-2} C_2 C_0 C_2^{\top}$ $C_4 = C_0 - C_3$ $C_{5i} = -w_i C_0 \mathbf{y}_i \mathbf{y}_i^{\top} C_0$ $C_{6i} = C_1^{-1} C_2 C_{5i} + C_1^{-1} C_{5i} C_2^{\top} - C_1^{-2} C_2 C_{5i} C_2^{\top}$ $C_{7i} = C_{5i} - C_{6i}$ $C_{8i} = -2\tilde{l}_i w_i^{1/2} C_1^{-1/2} C_0 \mathbf{y}_i \boldsymbol{\alpha}^{\top} + \tilde{l}_i w_i^{1/2} C_1^{-3/2} C_2 C_0 \mathbf{y}_i \boldsymbol{\alpha}^{\top}$ $C_{9i} = 2\tilde{l}_i w_i^{1/2} C_0 \mathbf{y}_i \boldsymbol{\delta}^{\top} C_0$ $C_{10i} = C_1^{-1} C_2 C_{9i} + C_1^{-1} C_{9i} C_2^{\top} - C_1^{-2} C_2 C_{9i} C_2^{\top}$ $C_{11i} = C_{8i} + C_{9i} - C_{10i}$ $C_{12i} = 2\tilde{l}_i^2 C_1^{(-1/2)} \boldsymbol{\alpha} \boldsymbol{\delta}^{\top} C_0 - \tilde{l}_i^2 C_1^{-3/2} \boldsymbol{\alpha} \boldsymbol{\delta}^{\top} C_0 C_2^{\top}$ $C_{13i} = -\tilde{l}_i^2 C_0 \boldsymbol{\delta} \boldsymbol{\delta}^{\top} C_0$ $C_{14i} = C_1^{-1} C_2 C_{13i} + C_1^{-1} C_{13i} C_2^{\top} - C_1^{-2} C_2 C_{13i} C_2^{\top}$ $C_{15i} = C_{12i} + C_{13i} - C_{14i}$ $V_1 = \text{diag}(V)^{-1/2}$ $V_2 = \text{diag}(V)^{-3/2}$	$\nabla_{\alpha} \log p(\boldsymbol{\theta}, \tilde{\mathbf{l}}, \mathbf{w} \mathbf{y})$ $= \nabla_{\alpha} \left\{ -\frac{n}{2} T_{\alpha 1} - \frac{1}{2} \sum_{i=1}^n (T_{\alpha 2i} + T_{\alpha 3i} + T_{\alpha 4i}) \right\}$ $+ \nabla_{\alpha} \log p(\boldsymbol{\alpha})$ $\nabla_{\alpha} T_{\alpha 1} = 2C_1^{-3/2} \bar{\Omega} \boldsymbol{\alpha} \boldsymbol{\alpha}^{\top} \bar{\Omega} C_0 \boldsymbol{\delta} - 2C_1^{-1/2} \bar{\Omega} C_0 \boldsymbol{\delta}$ $\nabla_{\alpha} T_{\alpha 2i} = C_1^{-2} \bar{\Omega} \boldsymbol{\alpha} \boldsymbol{\alpha}^{\top} \bar{\Omega} (C_{5i} + C_{5i}^{\top}) \bar{\Omega} \boldsymbol{\alpha}$ $- C_1^{-1} \bar{\Omega} (C_{5i} + C_{5i}^{\top}) \bar{\Omega} \boldsymbol{\alpha}$ $\nabla_{\alpha} T_{\alpha 3i} = C_{16i} + C_1^{-1} \bar{\Omega} (C_{17i} + C_{17i}^{\top}) \bar{\Omega} \boldsymbol{\alpha}$ $- C_1^{-2} \bar{\Omega} \boldsymbol{\alpha} \boldsymbol{\alpha}^{\top} \bar{\Omega} (C_{17i} + C_{17i}^{\top}) \bar{\Omega} \boldsymbol{\alpha}$ $\nabla_{\alpha} T_{\alpha 4i} = 2C_{18i} + C_1^{-1} \bar{\Omega} (C_{19i} + C_{19i}^{\top}) \bar{\Omega} \boldsymbol{\alpha}$ $- C_1^{-2} \bar{\Omega} \boldsymbol{\alpha} \boldsymbol{\alpha}^{\top} \bar{\Omega} (C_{19i} + C_{19i}^{\top}) \bar{\Omega} \boldsymbol{\alpha}$ $\nabla_{\alpha} \log p(\boldsymbol{\alpha}) = -\frac{1}{\sigma^2} \sum_i \alpha_i$ $C_{16i} = -2\tilde{l}_i w_i^{1/2} C_1^{-1/2} \bar{\Omega} C_0 \mathbf{y}_i$ $+ 2\tilde{l}_i w_i^{1/2} C_1^{-3/2} \boldsymbol{\alpha}^{\top} \bar{\Omega} C_0 \mathbf{y}_i \bar{\Omega} \boldsymbol{\alpha}$ $C_{17i} = -2\tilde{l}_i w_i^{1/2} C_0 \mathbf{y}_i \boldsymbol{\delta}^{\top} C_0$ $C_{18i} = \tilde{l}_i^2 C_1^{-1/2} \bar{\Omega} C_0 \boldsymbol{\delta} - \tilde{l}_i^2 C_1^{-3/2} \bar{\Omega} \boldsymbol{\alpha} \boldsymbol{\alpha}^{\top} \bar{\Omega} C_0 \boldsymbol{\delta}$ $C_{19i} = \tilde{l}_i^2 C_0 \boldsymbol{\delta} \boldsymbol{\delta}^{\top} C_0$
Computing $\nabla_{\tilde{G}} \log p(\boldsymbol{\theta}, \tilde{\mathbf{l}}, \mathbf{w} \mathbf{y})$	Computing $\nabla_{\tilde{\nu}} \log p(\boldsymbol{\theta}, \tilde{\mathbf{l}}, \mathbf{w} \mathbf{y})$
$\nabla_{\tilde{G}} \log p(\boldsymbol{\theta}, \tilde{\mathbf{l}}, \mathbf{w} \mathbf{y}) = \nabla_G \log p(\boldsymbol{\theta}, \tilde{\mathbf{l}}, \mathbf{w} \mathbf{y}) \times \exp(\tilde{G}) + 1$	$\nabla_{\tilde{\nu}} \log p(\boldsymbol{\theta}, \tilde{\mathbf{l}}, \mathbf{w} \mathbf{y})$ $= \nabla_{\nu} \left\{ \mathcal{L}(\mathbf{y}, \tilde{\mathbf{l}}, \mathbf{w} \boldsymbol{\theta}) + \log(p(\nu)) \right\} \times \exp(\tilde{\nu}) + 1$ $\nabla_{\nu} \mathcal{L}(\mathbf{y}, \tilde{\mathbf{l}}, \mathbf{w} \boldsymbol{\theta}) = \frac{1}{2} \sum_{i=1}^n \log(w_i)$ $+ n \left( \frac{1}{2} \log\left(\frac{\nu}{2}\right) + \frac{1}{2} - \frac{1}{2} \psi_0\left(\frac{\nu}{2}\right) \right) - \frac{1}{2} \sum_{i=1}^n w_i$ $\nabla_{\nu} \log(p(\nu)) = (a_2 - 1) \frac{1}{\nu} - b_2$

Note: the gradient is computed by evaluated the terms sequentially from the bottom upwards.



---

**Algorithm 1** Hybrid VI for AC Skew-t Copula

---

Initiate  $\boldsymbol{\lambda}^{(0)}$  and set  $t = 0$

**repeat**

- (a) Generate  $\boldsymbol{\theta}^{(t)}$  using its re-parametrized representation
- (b) Generate  $\{\tilde{\mathbf{l}}^{(t)}, \mathbf{w}^{(t)}\} \sim p(\tilde{\mathbf{l}}, \mathbf{w} | \boldsymbol{\theta}^{(t)}, \mathbf{y})$
- (c) Compute the gradient  $\widehat{\nabla_{\boldsymbol{\lambda}} \mathcal{L}}$  using (14) evaluated at the values  $\boldsymbol{\lambda}^{(t)}, \boldsymbol{\theta}^{(t)}$
- (d) Compute step size  $\boldsymbol{\rho}^{(t)}$  using an adaptive method (e.g. an ADA method)
- (e) Set  $\boldsymbol{\lambda}^{(t+1)} = \boldsymbol{\lambda}^{(t)} + \boldsymbol{\rho}^{(t)} \circ \widehat{\nabla_{\boldsymbol{\lambda}} \mathcal{L}}(\boldsymbol{\lambda}^{(t)})$
- (f) Set  $t = t + 1$

**until** either a stopping rule is satisfied or a fixed number of steps is taken

Set  $\widehat{\boldsymbol{\lambda}} = \frac{1}{100} \sum_{s=1}^{100} \boldsymbol{\lambda}^{(t+1-s)}$ , and the variational parameter posterior to  $q_{\widehat{\boldsymbol{\lambda}}}^0(\boldsymbol{\theta})$

---

from each of two skew-t factor copulas. The first case is a low-dimensional single factor model ( $d = 5, k = 1$ ; Case 1), and the second is higher dimensional five factor model ( $d = 30, k = 5$ ; Case 2). The copula parameters were obtained from fitting these models to the returns data; see Part B of the Web Appendix for details of these two data generating processes.

## 4.2 Approximation accuracy

For both examples, the variational posterior is compared to the exact posterior  $p(\boldsymbol{\theta} | \mathbf{y})$  computed using the (slower) MCMC scheme in Appendix C. MCMC evaluates the posterior up to an arbitrary error, which we made small using a large Monte Carlo sample size. Estimation accuracy is measured using pairwise dependence metrics of the fitted skew-t copulas for all possible variable pairs. These metrics include the quantile dependencies computed at the 1% and 5% quantiles, and the Spearman correlation. For the pair  $(Y_i, Y_j)$ , the latter is  $\rho_{ij}^S = 12 \int \int C_{ij}(u'_i, u'_j) du'_i du'_j - 3$ , with  $C_{ij}$  the bivariate marginal copula for  $(Y_i, Y_j)$  from the skew-t copula evaluated as in Appendix A.

The exact and approximate posterior means of the metrics are evaluated by averaging their values computed at Monte Carlo draws from  $p(\boldsymbol{\theta} | \mathbf{y})$  and  $q_{\widehat{\boldsymbol{\lambda}}}^0(\boldsymbol{\theta})$ , respectively. Figure 2 plots the exact and variational posterior means of the pairwise Spearman correlations. Figures 3 and 4 do the same for the quantile dependence metrics at the 5% level. They show that VI produces a copula estimate with a dependence structure that is close to that of the exact posterior; further results are given in Part B of the Web Appendix.

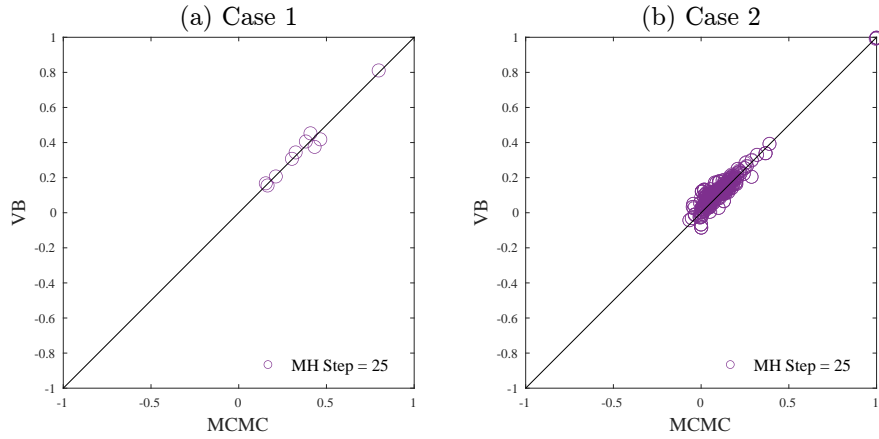


Figure 2: Comparison of the posterior mean estimates of the pairwise Spearman correlations  $\rho_{ij}^S$  computed exactly using MCMC (horizontal axis) and approximately using VI (vertical axis). Panel (a) plots these for the 5-dimensional skew-t copula in Case 1, and panel (b) for the 30-dimensional skew-t copula in Case 2.

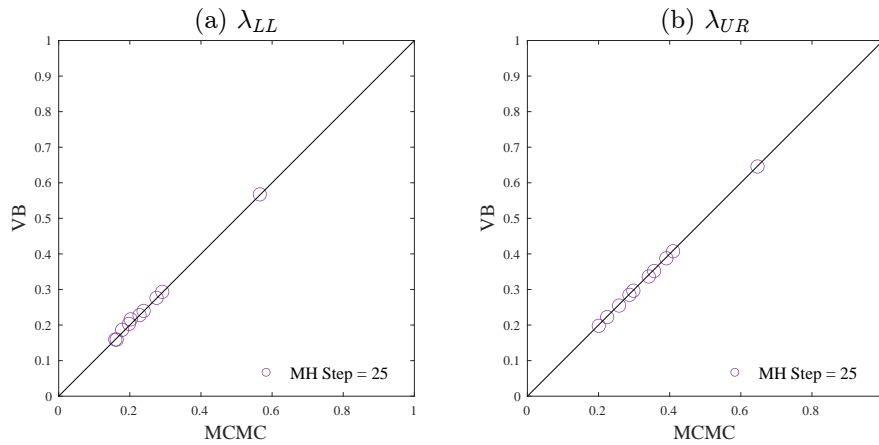


Figure 3: Comparison of the posterior mean estimates of the pairwise 5% quantile dependence metrics  $\lambda_{LL}(0.05)$  and  $\lambda_{UR}(0.05)$  for Case 1 computed exactly using MCMC (horizontal axis) and approximately using VI (vertical axis).

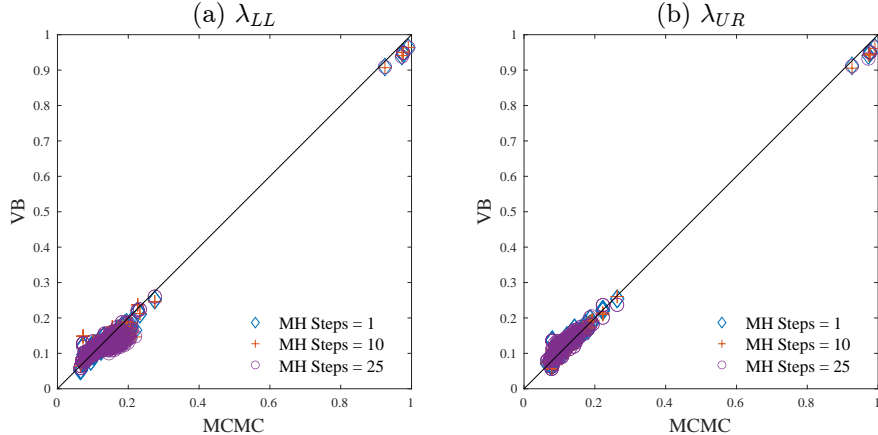


Figure 4: Comparison of the posterior mean estimates of pairwise metrics  $\lambda_{LL}(0.05)$  and  $\lambda_{UR}(0.05)$  for Case 2 computed exactly using MCMC (horizontal axis) and approximately using VI (vertical axis). Results are given for three VI implementations where 1, 10 and 25 random walk Metropolis-Hastings draws were used at step (b) of Algorithm 1.

### 4.3 Approximation speed

Algorithm 1 is implemented using random walk Metropolis-Hastings (MH) with 25 draws at step (b) throughout. To illustrate that the algorithm is robust to the number of draws, Figure 4 plots estimates for three implementations with 1, 10 and 25 MH draws. The VI estimates are very similar, which is consistent with the finding of Loaiza-Maya et al. (2022) for very different models.

Table 2 compares the computation time for MCMC and VI (with 25 MH draws) using a low-end laptop. The diagnostic of Geweke (1991) was used to determine the number of MCMC sweeps required. The number of steps in the SGA algorithm was 5000, which is a conservative number as judged by the stability of the optimal VA; for example, in Case 1 the VA based on only 2500 steps is very similar. The VI estimator is faster, and its computational advantage grows with  $d$  and  $k$ .

### 4.4 Choice of data augmentation

Our approach uses the generative representation at (6) (labelled ‘GR3’) to construct a variational data augmentation method. One drawback is that a nested (albeit fast) MCMC sampler to draw from  $p(\tilde{\mathbf{l}}, \mathbf{w} | \boldsymbol{\theta}, \mathbf{y})$  is required at step (b) of Algorithm 1. However, the alternative generative representation ‘GR1’ in Appendix B with latent vector  $\mathbf{l} = (l_1, \dots, l_n)^\top$  can also be used. The corre-

Table 2: Computation times to estimate skew-t copulas for simulated datasets

Case 1 (Dimension $d = 5$ with $k = 1$ Factor)			
	Time/Step (seconds)	Number of Steps	Total Time (hours)
MCMC	0.207	27000	1.553
VB	0.268	5000	0.372
Case 2 (Dimension $d = 30$ with $k = 5$ Factors)			
MCMC	1.580	33000	14.480
VB	1.446	5000	2.008

Note: Computation times in MATLAB for a MacBook Pro (with 2.3GHz Intel i5 CPU) laptop.

sponding hybrid VI algorithm targets  $p(\mathbf{l}, \boldsymbol{\theta} | \mathbf{y})$ , where at step (b) direct generation from  $p(\mathbf{l} | \boldsymbol{\theta}, \mathbf{y})$  is possible without the use of a nested MCMC sampler. However, we found application of the SGA algorithm to be less efficient for GR1; see Part C of the Web Appendix for empirical illustration.

## 5 Analysis of Intraday Financial Returns

We use the AC skew-t copula, fitted using the proposed VI method, to capture asymmetric dependence in two examples using high frequency intraday financial data. The first illustrates the flexibility of the dependence structure of this copula by considering the returns on two equities and the VIX index. The second is our main example and uses the copula to capture the dependence between the returns on 93 equities. The focus is on the pairwise tail dependence estimates, which are heterogeneous across equity pairs, along with predictive accuracy and portfolio construction. In both examples, we follow Patton (2006) and many others by using the copula to capture cross-sectional dependence in the conditional distribution of the financial variables. We first describe the data and the marginal model for the intraday equity returns, followed by the two empirical studies.

### 5.1 Data Description and Marginal Model

The trade prices of the constituents of the S&P100 index as of 31 Dec. 2021 were obtained from Revinitiv DataScope Select database, for the period 1 Jan. 2017 to 31 Dec. 2021. Only the 93

equities that are listed over the entire period are used in our empirical analysis. For a given equity, the  $N = 26$  fifteen minute returns between 09:30 and 16:00 EDT of each trading day are constructed as follows. If  $P_{\tau,t}$  denotes the last trade price of a given equity in the  $\tau$ th 15 minute interval on trading day  $t$ , then the return for that interval is  $r_{\tau,t} = \log(P_{\tau,t}) - \log(P_{\tau-1,t})$ , with  $P_{0,t} \equiv P_{N,t-1}$  the last trade price on the previous day. Days where trading is suspended are removed.

The intraday GARCH model of Engle and Sokalska (2012) is used as a marginal model for the returns on each equity, which decomposes the return into components

$$r_{\tau,t} = (h_t s_\tau)^{1/2} \sigma_{\tau,t} \varepsilon_{\tau,t}.$$

Here,  $h_t = \sum_{i=1}^N (r_{\tau,t})^2$  is the realized variance of day  $t$ ,  $s_\tau = \frac{1}{T} \sum_{t=1}^T (r_{\tau,t})^2 / h_t$  is an estimate of the diurnal pattern in volatility for the  $\tau$ th interval, and the conditional volatility movement

$$\sigma_{\tau,t}^2 = \beta_0 + \beta_1 \epsilon_{\tau-1,t}^2 + \beta_2 \sigma_{\tau-1,t}^2,$$

with  $\epsilon_{\tau,t} = r_{\tau,t} / (h_t s_\tau)^{1/2}$ ,  $\epsilon_{0,t} = \epsilon_{N,t-1}$  and  $\sigma_{0,t} = \sigma_{N,t-1}$ . In our analysis, we assume that the innovation  $\varepsilon_{\tau,t} \sim t_1(0, 1, \nu)$ , and estimate the parameters  $(\beta_0, \beta_1, \beta_2)$  for each equity using maximum likelihood. The copula data is computed as  $T(\varepsilon_{\tau,t}; \nu)$  at the model estimates.<sup>7</sup>

## 5.2 Asymmetric Dependence Between Equity Returns and the VIX

The first example applies the AC copula model with  $k = 1$  factor to two equity returns series and the VIX. The latter is a measure of overall market volatility published by the Chicago Board of Exchange (Britten-Jones and Neuberger, 2000) and 15 minute observations were obtained from Revinitiv DataScope Select database. The VIX marginal model is a first order autoregression with a nonparametric disturbance estimated using a kernel density estimator. The two equities are Bank of America (BAC) and JP Morgan (JPM). The copula model was fit to data from two periods of 40 trading days: a low volatility period between 24 Oct. and 22 Dec. 2017, and a high

<sup>7</sup>To match this with the copula model notation in Section 3.1, note that if  $i = (N-1)t + \tau$  (so that  $i = 1, 2, \dots, NT$ ) and the equity return is the  $j$ th marginal, then  $y_{ij} = r_{\tau,t}$  and  $F_{Y_j}(y_{ij}) = T(\varepsilon_{\tau,t}; \nu)$  in (8).

volatility period between 11 Feb. and 15 Apr. 2020.<sup>8</sup> Table 3 reports the estimates of the copula parameters, correlations and asymmetry measures. The two equity returns are positively correlated, whereas they are both negatively correlated with the VIX. There are also strong asymmetries in the pairwise dependencies, which change in direction and scale from the low to high volatility periods. For example, between the two equity returns,  $\Delta_{\text{Major}}(0.05)$  changes from 0.169 to  $-0.279$ . This suggests that during periods of high market volatility, negative returns are more dependent than positive returns.

Table 3: Estimated AC skew-t copula for the BAC-JPM-VIX example

Low Volatility Period (24 Oct. 2017—22 Dec. 2017)								
Pair	Correlation			Tail Asymmetry		Parameters ( $\theta$ )		
	Pearson	Spearman	Kendall	$\Delta_{\text{Major}}(0.05)$	$\Delta_{\text{Minor}}(0.05)$	$\rho$	$(\delta_1, \delta_2)$	$\nu$
BAC – VIX	-0.322 (0.029)	-0.322 (0.029)	-0.219 (-0.021)	0.003 (0.003)	-0.059 (0.023)	-0.459 (0.036)	0.987, -0.422 (0.041), (0.006)	
JPM – VIX	-0.355 (0.041)	-0.355 (0.041)	-0.242 (0.029)	0.000 (0.001)	-0.061 (0.013)	-0.484 (0.037)	0.829, -0.422 (0.034), (0.006)	25.77 (4.76)
JPM – BAC	0.759 (0.028)	0.759 (0.028)	0.566 (0.025)	0.169 (0.041)	0.000 (0.000)	0.881 (0.024)	0.829, 0.987 (0.034), (0.041)	
High Volatility Period (11 Feb. 2020—15 Apr. 2020)								
Pair	Correlation			Tail Asymmetry		Parameters ( $\theta$ )		
	Pearson	Spearman	Kendall	$\Delta_{\text{Major}}(0.05)$	$\Delta_{\text{Minor}}(0.05)$	$\rho$	$(\delta_1, \delta_2)$	$\nu$
BAC – VIX	-0.536 (0.024)	-0.536 (0.024)	-0.381 (0.019)	-0.019 (0.004)	0.240 (0.030)	-0.697 (0.023)	-0.987, 0.649 (0.004), (0.030)	
JPM – VIX	-0.547 (0.028)	-0.547 (0.028)	-0.393 (0.023)	-0.008 (0.002)	0.211 (0.019)	-0.708 (0.023)	-0.865, 0.649 (0.025), (0.030)	4.11 (0.34)
JPM – BAC	0.805 (0.023)	0.805 (0.023)	0.620 (0.024)	-0.279 (0.038)	-0.002 (0.001)	0.911 (0.017)	-0.865, -0.987 (0.025), (0.004)	

Note: The variational posterior means, along with standard deviations in parentheses below, of the correlation coefficients (Pearson, Spearman, and Kendall), 5% quantile asymmetry metrics defined in the text, and copula parameters are reported. Results are given for two windows of 40 days of 15 minute data that correspond to low and high market volatility periods as discussed in the text.

Figures 5 and 6 further summarize the dependence structure of the estimated copula for the low and high market volatility periods, respectively. Following Oh and Patton (2013), panels (d,g,h) give “quantile dependence plots” for the pairs BAC-VIX, JPM-VIX and JPM-BAC, respectively. These visualize asymmetric dependence along the major diagonal by plotting the quantile dependencies  $\lambda_{\text{LL}}(u)$  &  $\lambda_{\text{UR}}(1-u)$  against  $u$  (blue & red lines), and along the minor diagonal by plotting  $\lambda_{\text{LR}}(u)$

<sup>8</sup>The first period contains the lowest VIX value in our data, whereas the second contains the highest VIX value that corresponds to the COVID-19 crash.

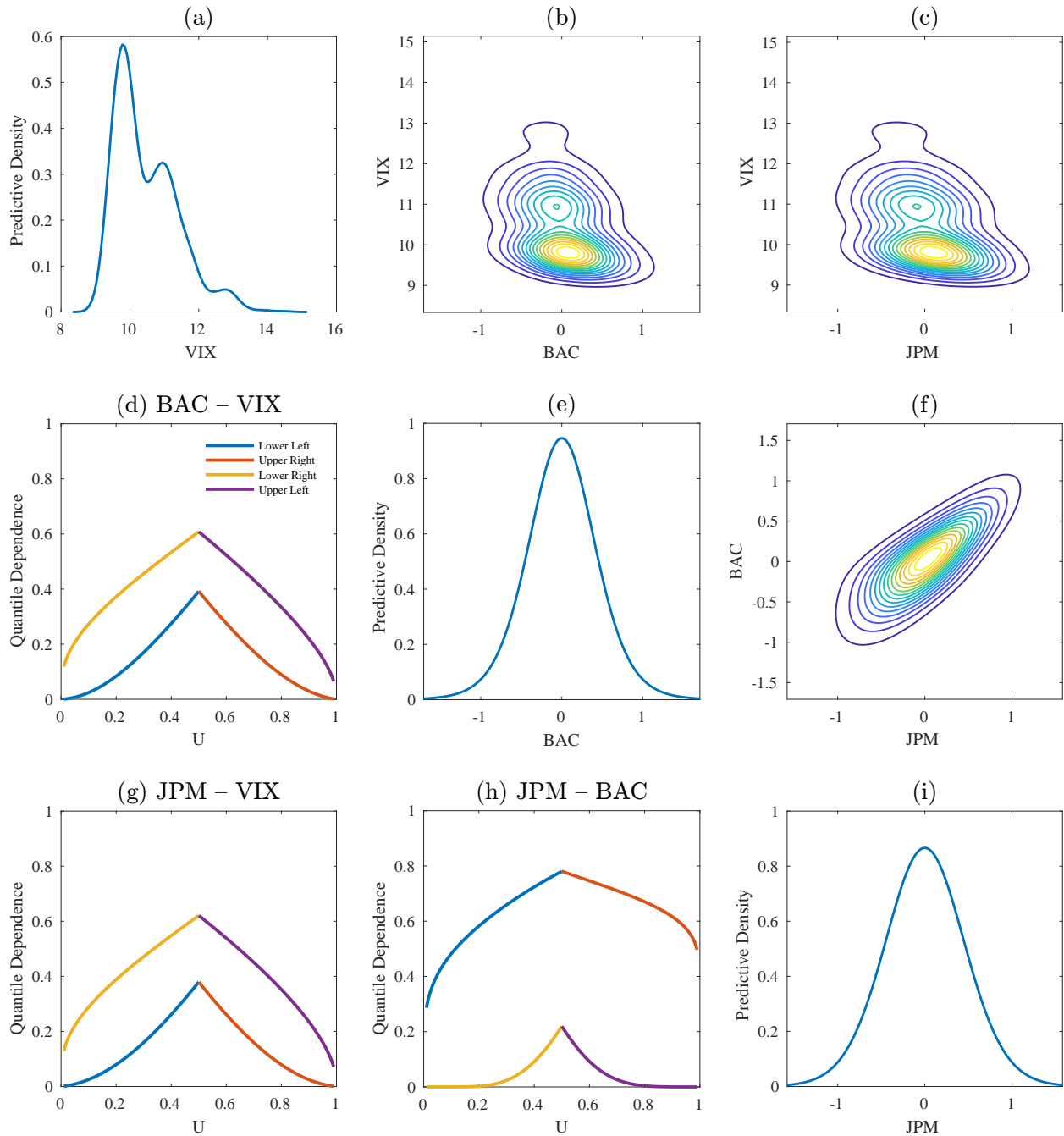


Figure 5: **Low Volatility Period** results from the AC Skew-t copula model for variables (VIX, BAC, JPM). Panels (a,e,g) give marginal predictive distributions for the series, and panels (b,c,f) give bivariate predictive distributions for the variable pairs, all on 23 Dec. 2017 at 09:45. Estimated quantile dependence plots for the pairs are given in panels (d) JPM-VIX, (g) BAC-VIX, and (h) JPM-BAC. Each quantile dependence plot visualizes asymmetry along the major diagonal by plotting  $\lambda_{LL}(u)$  &  $\lambda_{UR}(1-u)$  against  $u$  (blue & red lines), and along the minor diagonal by plotting  $\lambda_{LR}(u)$  &  $\lambda_{UL}(1-u)$  versus  $u$  (yellow & purple lines).

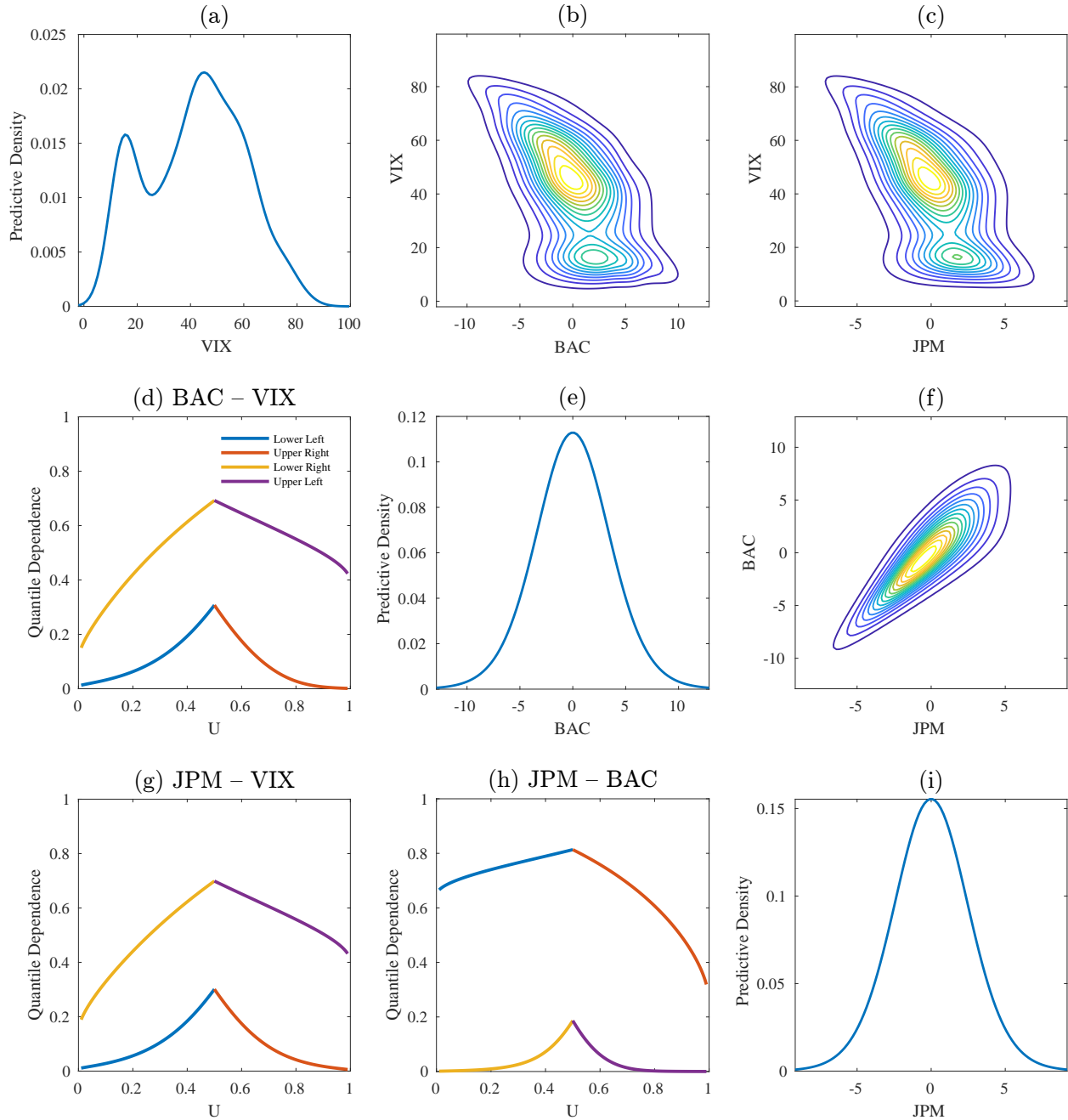


Figure 6: **High Volatility Period** results from the AC Skew-t copula model for variables (JPM, BAC, VIX). Panels (a,e,g) give marginal predictive distributions for the series, and panels (b,c,f) give bivariate predictive distributions for the variable pairs, all on 16 Apr. 2020 at 09:45. Estimated quantile dependence plots for the pairs are given in panels (d) JPM–VIX, (g) BAC–VIX, and (h) JPM–BAC. Each quantile dependence plot visualizes asymmetry along the major diagonal by plotting  $\lambda_{LL}(u)$  &  $\lambda_{UR}(1-u)$  versus  $u$  (blue & red lines), and along the minor diagonal by plotting  $\lambda_{LR}(u)$  &  $\lambda_{UL}(1-u)$  versus  $u$  (yellow & purple lines).



&  $\lambda_{UL}(1 - u)$  versus  $u$  (yellow & purple lines). The dependence between the two equity returns in the major diagonal is positively asymmetric during the low volatility period in Fig. 5(h), and negatively asymmetric during the high volatility period in Fig. 6(h). In contrast, dependence in the minor diagonal between the returns on both equities and the VIX is close to symmetric in the low volatility period in Fig. 5(d,g), but positively asymmetric during the high volatility period in Fig. 6(d,g), as also indicated by the asymmetry measures in Table 3.

To further visualize the flexibility of the copula model, we compute the predictive distribution of the three variables for the first 15-minute trading interval of the following day of each sample, which are 23 Dec. 2017 (low volatility period) and 16 Apr. 2020 (high volatility period). Figures 5 and 6 plot the marginal predictive densities in panels (a,e,i), and the bivariate slices of the joint predictive density in panels (b,c,f). In the high volatility period both the tails and asymmetric dependence of the distributions are greatly accentuated, compared to the low volatility period.

### 5.3 S&P100 Portfolio

We now apply the skew-t copula model to the 15 minute returns on all  $d = 93$  constituents of the S&P100 index in our data, which is our main application. Rolling windows of width  $T = 40$  trading days are used, so that the copula model is estimated using  $n = 26 \times 40 = 1040$  observations in each window. The model is re-fit every 20 trading days, resulting in 60 overlapping windows. Our empirical study focuses on three research issues. The first is whether adopting the AC skew-t copula improves the accuracy of 15-minute ahead density forecasts of portfolio returns, relative to benchmarks. The second is measuring the degree of asymmetric dependence—the main rationale of adopting the AC skew-t copula—over the five year period of our data. The third issue is whether, or not, exploiting asymmetry in dependence when forming investment portfolios can improve returns.

#### 5.3.1 Density forecasting

We consider 15 minute (i.e. one-step-ahead) density forecasts of the return on a market value weighted portfolio of the equities. The weights are re-calculated at the same frequency as the

model estimation—i.e. every 20 trading days—using market capitalization data sourced from the Center for Research in Security Prices (CRSP) database. However, forecasts are evaluated using the Bayesian posterior predictive distributions for every 15 minute period from 3 Mar. 2017 to 25 Jan. 2022, giving a total of  $1200 \times 26 = 31,200$  density forecasts. Each of these is evaluated by drawing 10,000 iterates from the posterior predictive joint distribution of returns (see Part D of the Web Appendix for details), from which draws of the portfolio return are computed. Kernel density estimates of these are an estimate of the posterior predictive distribution of the portfolio return.

Table 4: Mean log-score and CRPS values of 15 minute 93 Equity (S&P100 portfolio return predictions).

# Copula Factors $k$	Panel A: Mean Log-Score				Panel B: Mean CRPS			
	# Variational Factors $r$				Variational Factor $r$			
	0	3	5	10	0	3	5	10
1	6.097	6.179	6.111	6.325	8.468	8.462	8.456	8.404
3	6.856	6.744	6.853	6.890	8.334	8.344	8.345	8.307
5	7.106	7.131	7.117	7.106	8.277	8.276	8.254	8.285
10	7.156	<b>7.185</b>	7.132	7.167	8.251	<b>8.246</b>	8.252	8.288
15	7.132	7.174	7.143	7.193	8.246	8.246	8.246	8.248

Note: LS values are multiplied by 10, and CRPS values are multiplied by 100, for presentation. The means are computed over all 15 minute periods between 03/03/2017 and 25/01/2020.

Two density forecasting metrics are calculated: the log-score (LS) and the continuous ranked probability score (CRPS) of Gneiting et al. (2007). Higher values of the LS and lower values of the CRPS correspond to increased accuracy. Table 4 reports the mean of these over all portfolio return density forecasts. Results are given for different numbers of factors  $k$  in the copula model, and estimated using VI where the covariance matrix of the Gaussian VA  $q_\lambda^0$  has different numbers of factors  $r$ . Note that while setting  $r = 0$  corresponds to a fully factorized VA for  $q_\lambda^0$ , we stress that the VA  $q_\lambda$  at (12) for the target density  $p(\psi|\mathbf{y})$  is not of a mean field type. We make two observations. First, using higher values of  $k$  (i.e.  $k = 10$  and  $k = 15$ ) increases accuracy. This result is consistent with Oh and Patton (2023), who found latent group factors, over-and-above a single global factor, improve the dependence structure in their skew-t copula model. Second, the results

are similar for  $r = 3, 5, 10$ , which is consistent with Ong et al. (2018) and subsequent authors who find lower values of  $r$  typically work well. We focus on results for  $k = 10$  factors, which is the more parsimonious of the two best performing factor copulas, with  $r = 3$  for the VA.

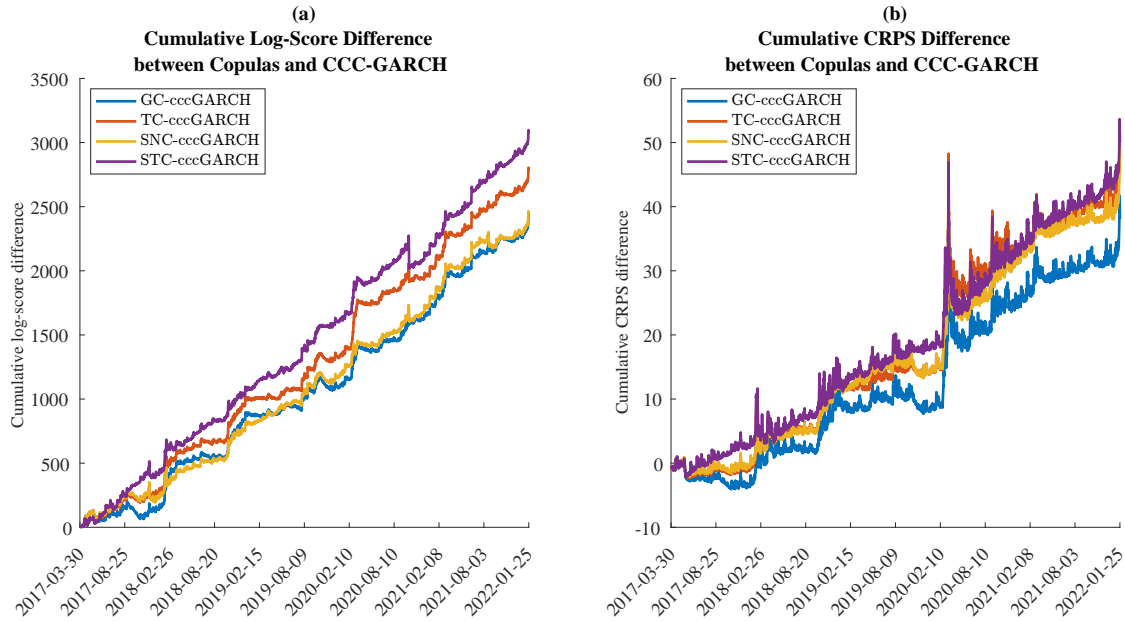


Figure 7: Cumulative difference in CRPS and LS scores between each of (i) Skew-t Copula, (ii) Skew-Normal Copula, (iii) t-Copula, and (iv) Gaussian Copula and the baseline CCC-GARCH models.

The predictive accuracy of the AC skew-t copula model is compared with four benchmark models. The first three are copula models with the same marginals, but copulas that are sub-types of the AC skew-t copula; namely, the AC skew-normal copula ( $\nu \rightarrow \infty$ ), the t-copula ( $\delta = \mathbf{0}$ ), and the Gaussian copula ( $\nu \rightarrow \infty$  and  $\delta = \mathbf{0}$ ). The fourth benchmark model is an intraday Constant Conditional Correlation GARCH (CCC-GARCH) (Bollerslev, 1990) specified as in Section 5.1, but with  $\varepsilon_{\tau,t} \sim N(0,1)$  and cross-asset correlation estimated using the sample correlation.

We treat the CCC-GARCH model as the baseline, and compute the cumulative difference of each metric for each copula model and this baseline model. Figure 7 plots the differences over the validation period for (a) LS and (b) CRPS. The values are positive, so that the four copula models all out-perform the baseline model, and the skew-t copula dominates the other copula models.

### 5.3.2 Asymmetric dependence

We compute the following metric of pairwise total asymmetric dependence,

$$\mathcal{T}_{i,j} = \int_{\epsilon}^{0.5} |\Delta_{\text{Major}}(u)| du, \quad (15)$$

where we set  $\epsilon = 0.001$  and compute the integral numerically. Asymmetry along the major diagonal is measured, rather than the minor diagonal, because most equity pairs exhibit positive overall dependence. When dependence is symmetric  $\mathcal{T}_{i,j} = 0$ , while the maximum value of the metric for the AC skew-t copula can be computed as  $\max_{\rho,\delta}\{\mathcal{T}_{i,j}\} = 0.193$  with  $\nu = 2$ .

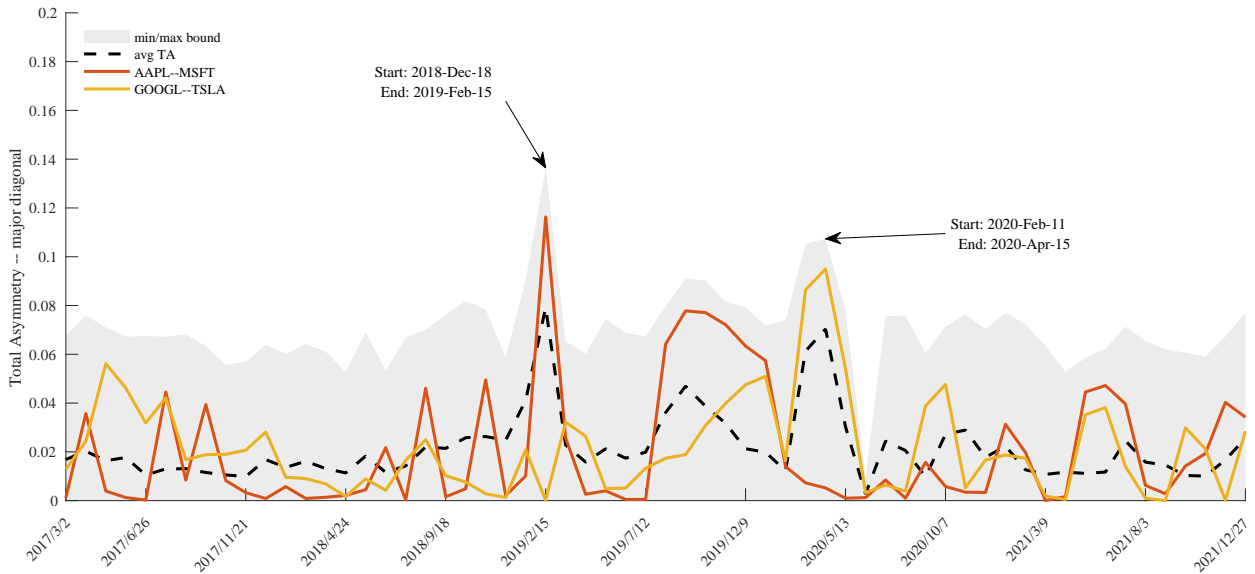


Figure 8: Summary of the total asymmetry metric values  $\mathcal{T}_{i,j}$  over the rolling windows in the five year period. The gray shaded area is the interval between  $\min_{i,j}\{\mathcal{T}_{i,j}\}$  and  $\max_{i,j}\{\mathcal{T}_{i,j}\}$ , while the dashed black line depicts the mean value across all equity pairs. The values of  $\mathcal{T}_{i,j}$  for the pairs Apple–Microsoft and Google–Tesla are plotted in red and orange, respectively.

This metric is computed for all  $93 \times 92/2 = 4278$  pairs of equities and for the AC skew-t copulas fitted at each of the 60 windows. Figure 8 summarizes the evolution of the  $\mathcal{T}_{i,j}$  values over the estimation windows as follows. The gray shaded area is the interval between  $\min_{i,j}\{\mathcal{T}_{i,j}\}$  and  $\max_{i,j}\{\mathcal{T}_{i,j}\}$ , while the dashed black line depicts the mean value across all equity pairs. The windows with the highest level of total asymmetry are 18 Dec. 2018 to 15 Feb. 2019, and 11 Feb. 2020 to 15 Apr. 2020. The former window corresponds to an escalating trade war between the U.S. and China, while the second window corresponds to the height of the COVID-19 equity

market crash. The  $\mathcal{T}_{i,j}$  values for the two pairs Apple–Microsoft and Google–Tesla are also plotted, illustrating how the level of asymmetric dependence can vary for different equity pairs.

Finally, to further highlight the heterogeneity in asymmetric tail dependence, Figure 9 depicts  $\Delta_{\text{Major}}(0.01)$  over the final ten non-overlapping windows across the ten equity pairs with the largest market capitalization. Positive values of  $\Delta_{\text{Major}}(0.01)$  (green) indicate upside tail dependence, while negative values of  $\Delta_{\text{Major}}(0.01)$  (red) indicate downside tail dependence. In particular, during the early stages of the COVID-19 crash in panel (h), the copula captures extreme downside tail dependence across all equity pairs, with the exception of Apple. Further summaries of tail dependence for more equities can be found in Part D of the Web Appendix.

### 5.3.3 Portfolio equity selection

Dependence between equity returns is one of the major attributes of asset selection strategies for investment portfolios. Traditionally, equities that are negatively correlated are preferred because they achieve a superior efficient investment frontier (Markowitz, 1952, Fabozzi et al., 2008). More recently, consideration has been given to “tail risk” of extreme downside losses. For example, Guidolin and Timmermann (2008) and Harvey et al. (2010) proposed portfolio selection based on skewness and/or kurtosis, Giacometti et al. (2021) propose a portfolio allocation strategy with penalty terms based on tail risk measures, Zhao (2021) proposes a new portfolio optimization method using a bivariate peak-over-threshold approach; and Bollerslev et al. (2022) made use of semi-beta risk measures, separating market upside and downside movements, for portfolio construction. We consider using pairwise tail dependencies from the copula to construct portfolios.

The following two strategies are considered to select five equity pairs from the 4278 possible:

- *Upside Gains*: to maximize upside gains, equities that move together strongly in the upper tail are preferred, so that equity pairs with the largest values of  $\Delta_{\text{Major}}(0.05)$  selected.
- *High Minor Tail Dependence*: to maximize negative dependence in the tails, equity pairs that maximize the sum of the minor diagonal tail dependencies,  $\lambda_{UL}(0.05) + \lambda_{LR}(0.05)$ , are selected.

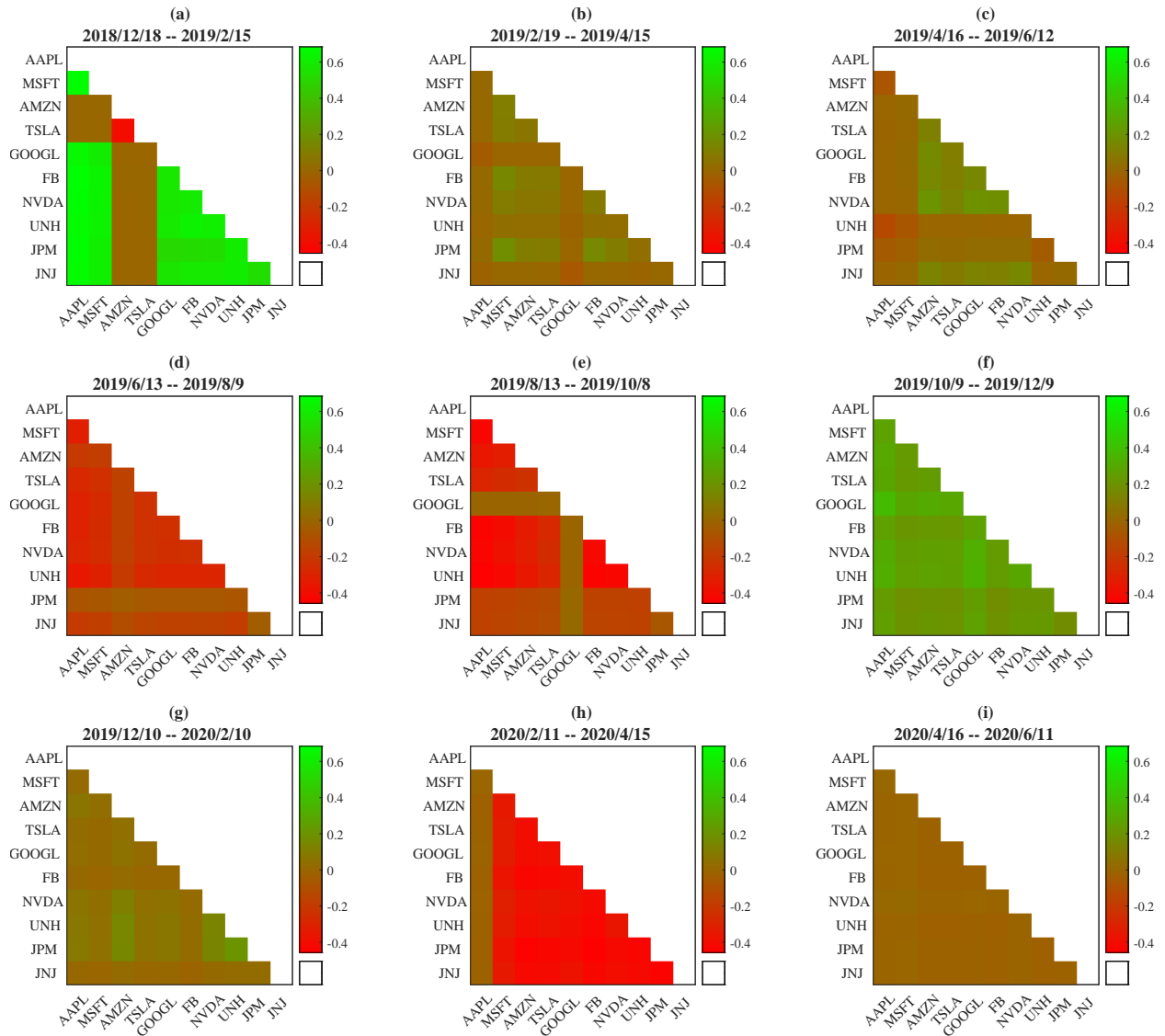


Figure 9: Heatmap of  $\Delta_{\text{Major}}(0.01)$  across the ten equity pairs with largest market capitalization between 18 December 2018 and 19 August 2020.

The equities that make up the top five pairs according to both criteria are used to construct portfolios using market-value weights.

Table 5 reports backtesting results from our equity selection strategies implemented for the period from 3 Mar. 2017 to 25 Jan. 2022. For comparison, we also report the market-value weighted portfolio with all 93 equities (i.e. the S&P100 index corrected for sample selection), along with a selection strategy based on the five equity pairs with the most negative Pearson’s correlation, as our benchmarks. All strategies are re-balanced with the most current statistics and market values every 20 trading days. The high minor tail dependence strategy performs strongly, even against the benchmark S&P100 portfolio. It has the highest Sharpe ratio and largest Value-at-Risk (VaR) at the 5% level.<sup>9</sup> While we stress that this study does not incorporate any trading costs, it suggests that trading strategies based on tail dependencies from our skew-t copula model have the potential to improve the risk profile—particularly tail risk—in portfolio selection.

Table 5: Backtesting results of the equity selection strategies.

	93 Equities (Benchmark S&P100)	Pearson’s Correlation (largest negative)	Upside Gain ( $\max \Delta_{\text{Major}}(0.05)$ )	High Minor Tail Depend. ( $\max \lambda_{UL}(0.05) + \lambda_{LR}(0.05)$ )
Sharpe Ratio	0.293	0.159	0.248	0.381
Return (p.a.)	15.736%	12.695%	17.443%	26.204%
Stdev (p.a.)	15.087%	22.449%	19.759%	19.327%
VaR(95%)	-6.054%	-8.064%	-7.633%	-5.804%

We report the Sharpe ratio, annualized realized portfolio return and standard deviation, and the 95% Value-at-Risk. The portfolio 93 Equities is the S&P 100 portfolio corrected for stock selection.

## 6 Discussion

In this paper we suggest that an AC skew-t factor copula is an attractive choice for modeling the dependence in large panels of financial data. Estimation in high dimensions is difficult, and we propose a new fast and accurate variational inference method to do so. A major empirical finding of the study is to show that not only is asymmetric tail dependence present in financial data, it can vary substantially over variable pairs. Capturing this in intraday equity returns increases the

<sup>9</sup>The risk-free rate used in the calculation of the Sharpe Ratio is the Federal Reserve Effective Rate, obtained from the St. Louis FRED database.

accuracy of density forecasts, and stock selection strategies based on the tail dependencies can perform well. Below, we conclude with some additional comments on the method and model.

While Bayesian VI methods are growing popularity in econometrics (see Loaiza-Maya and Nibbering (2022), Chan and Yu (2022) and Gefang et al. (2023) for some examples) for more complex models, the choice of both target and approximating densities is crucial. For the skew-t copula, the posterior  $p(\boldsymbol{\theta}|\mathbf{y})$  has a complex geometry, so that it is difficult to approximate directly and standard VI methods do not work well. However, we show that the augmented posterior based on a generative representation is tractable and well approximated using (12).

Previous studies use dynamic factors to model multiple years of daily or weekly asset returns. In our study of high frequency intraday returns we instead use a rolling window of width 40 trading days, and do not adopt a dynamic copula specification. For studies of lower frequency returns, allowing for time variation in the AC skew-t copula may be achieved by following previous authors and adopting a dynamic specification for the factors. When estimating any implicit copula, it is necessary to compute the marginal quantile functions  $F_{Z_j}^{-1}$  for each  $j = 1, \dots, d$  and at every observation (Smith, 2021). For the GH skew-t distribution this difficult and very large Monte Carlo samples (e.g. 1 million draws) are typically used to compute them to a necessary level of accuracy. One way to speed this computation is to set  $\boldsymbol{\delta} = \delta(1, 1, \dots, 1)^\top$  as in Oh and Patton (2023), however this restricts the degree of heterogeneity in the pairwise asymmetric dependencies, which is the key focus of our study. In contrast, the marginal quantile functions of the Azzalini and Capitanio (2003) distribution can be computed with very high accuracy using fast methods (Yoshihara, 2018), so that restricting the skew parameters  $\boldsymbol{\delta}$  is unnecessary. In a final comment, we observe that most previous factor copula studies use only one or two global factors, often enriched with an industry or latent group-specific factor. An advantage of the computational efficiency of the proposed VI method is that it allows for a larger number of global factors to be used. In our empirical work we find 10–15 global factors improves out-of-sample predictive performance, compared to a smaller number. This rich factor structure and the unrestricted skewness parameter vector gives estimates of tail dependencies from the copula that can be used to select portfolios with strong performance.



## Appendix A Quantile Dependence

For each skew-t copula, the pairwise quantile dependence metrics in Section 2.3 are evaluated from their bivariate copula function  $C(u_1, u_2) = F_{Z_1, Z_2} \left( F_{Z_1}^{-1}(u_1), F_{Z_2}^{-1}(u_2) \right)$ . Computation of  $F_{Z_j}^{-1}(u_j)$  is discussed in the manuscript for each distribution. The function  $F_{Z_1, Z_2}$  is obtained for the SDB skew-t distribution by numerical integration. For the AC skew-t distribution it is computed as the trivariate student t distribution function  $F_{Z_{AC}} \left( (z_1, z_2)^\top; \boldsymbol{\delta}, \bar{\boldsymbol{\Omega}}, \nu \right) = 2F_t \left( (z_1, z_2, 0)^\top; \boldsymbol{\Omega}^*, \nu \right)$ , where

$$\boldsymbol{\Omega}^* = \begin{pmatrix} \bar{\boldsymbol{\Omega}} & -\boldsymbol{\delta} \\ -\boldsymbol{\delta}^\top & 1 \end{pmatrix},$$

which can be derived from (4). The GH skew-t distribution function cannot be computed in closed form, and numerical integration of its joint density is difficult. Therefore, a kernel-based approximation based on one million Monte Carlo draws is employed.

## Appendix B Generative Representations for AC Skew-t

We list below three different generative representations for  $\mathbf{Z}_{AC}$  that can be derived from (4).

GR1: The first is to generate from the marginal  $L \sim t_1(0, 1, \nu)$  constrained so that  $L > 0$ , and then

$$\text{from the conditional } \mathbf{Z}_{AC} = (\mathbf{X}|L) \sim t_d \left( \mathbf{0}, \frac{\nu+L^2}{\nu+1} (\bar{\boldsymbol{\Omega}} - \boldsymbol{\delta}\boldsymbol{\delta}^\top), \nu+1 \right).$$

GR2: The second uses a scale mixture of normals representation for a t-distribution, where if

$$W \sim \text{Gamma}(\nu/2, \nu/2), \text{ then } (\mathbf{X}^\top, L)^\top = W^{-1/2} (\tilde{\mathbf{X}}^\top, \tilde{L})^\top \text{ with } (\tilde{\mathbf{X}}^\top, \tilde{L})^\top \sim N_{d+1}(\mathbf{0}, \boldsymbol{\Omega}).$$

Thus, generate sequentially (i)  $W \sim \text{Gamma}(\nu/2, \nu/2)$ , then (ii) from the conditional  $L|W \sim N(0, 1/W)$  constrained so  $L > 0$ , and then (iii) from the conditional  $\mathbf{Z}_{AC} = (\mathbf{X}|L, W) \sim N_d(\boldsymbol{\delta}L, W^{-1}(\bar{\boldsymbol{\Omega}} - \boldsymbol{\delta}\boldsymbol{\delta}^\top))$ .

GR3: The third representation is similar to GR2, but exploits the identity  $(\mathbf{X}|L > 0) = (\mathbf{X}|\tilde{L} > 0)$

with  $\tilde{L} = W^{1/2}L$ . Thus, generate sequentially (i)  $W \sim \text{Gamma}(\nu/2, \nu/2)$ , then (ii) from  $\tilde{L} \sim N(0, 1)$  constrained so  $\tilde{L} > 0$ , and then (iii) from the conditional  $\mathbf{Z}_{AC} = (\mathbf{X}|\tilde{L}, W) \sim N_d \left( W^{-1/2}\boldsymbol{\delta}\tilde{L}, W^{-1}(\bar{\boldsymbol{\Omega}} - \boldsymbol{\delta}\boldsymbol{\delta}^\top) \right)$ .

The extended likelihood in Section 3.2 is based on generative representation GR3.

## Appendix C MCMC Scheme

Algorithm 2 is an MCMC sampling scheme to evaluate the augmented posterior of the AC skew- $t$  factor copula parameters  $\boldsymbol{\theta}$ . Steps 1 and 2 are also used in the hybrid VI Algorithm 1.

---

### Algorithm 2 MCMC Scheme for AC Skew- $t$ Copula

---

- Step 0. Initialize feasible values for  $\boldsymbol{\theta}$ ,  $\tilde{\boldsymbol{l}}$  and  $\boldsymbol{w}$
  - Step 1. Generate from  $p(\tilde{\boldsymbol{l}}|\boldsymbol{\theta}, \boldsymbol{w}, \boldsymbol{y}) = \prod_{i=1}^n p(\tilde{l}_i|\boldsymbol{\theta}, w_i, \boldsymbol{y}_i)$
  - Step 2. Generate from  $p(\boldsymbol{w}|\boldsymbol{\theta}, \tilde{\boldsymbol{l}}, \boldsymbol{y}) = \prod_{i=1}^n p(w_i|\boldsymbol{\theta}, \tilde{l}_i, \boldsymbol{y}_i)$
  - Step 3. Generate from  $p(\alpha_j|\{\boldsymbol{\theta}\setminus\alpha_j\}, \tilde{\boldsymbol{l}}, \boldsymbol{w}, \boldsymbol{y})$  for  $j = 1, \dots, d$ .
  - Step 4. Generate from  $p(\tilde{g}_{ij}|\{\boldsymbol{\theta}\setminus\tilde{g}_{ij}\}, \tilde{\boldsymbol{l}}, \boldsymbol{w}, \boldsymbol{y})$  for non-zero elements  $\tilde{g}_{ij}$  of  $\tilde{G}$ .
  - Step 5. Generate from  $p(\nu|\{\boldsymbol{\theta}\setminus\nu\}, \tilde{\boldsymbol{l}}, \boldsymbol{w}, \boldsymbol{y})$
- 

The conditional posteriors at Steps 3, 4 and 5 can each be derive from (11), but are unrecognizable.

Therefore we employ adaptive random walk Metropolis-Hastings schemes to generate each element.

To derive the posteriors at Steps 1 and 2, note that from (9) and (10),

$$\begin{aligned} p(\tilde{\boldsymbol{l}}, \boldsymbol{w}|\boldsymbol{\theta}, \boldsymbol{y}) &\propto p(\tilde{\boldsymbol{l}}, \boldsymbol{w}, \boldsymbol{y}|\boldsymbol{\theta}) \propto \prod_{i=1}^n p(\boldsymbol{z}_i|\tilde{l}_i, w_i, \boldsymbol{\theta})p(\tilde{l}_i|w_i)p(w_i|\nu) \\ &= \prod_{i=1}^n \phi_d(\boldsymbol{z}_i; \boldsymbol{\mu}_{z,i}, \Sigma_{z,i})\phi_1(\tilde{l}_i; 0, 1)\mathbb{1}(\tilde{l}_i > 0)p(w_i|\nu), \end{aligned}$$

with  $\boldsymbol{\mu}_{z,i} = \boldsymbol{\delta}\tilde{l}_i w_i^{-1/2}$ ,  $\Sigma_{z,i} = w_i^{-1}(\bar{\boldsymbol{\Omega}} - \boldsymbol{\delta}\boldsymbol{\delta}^\top)$  and  $p(w_i|\nu)$  is a Gamma( $\nu/2, \nu/2$ ) density.

From the above, at Step 1 the conditional posterior  $p(\tilde{\boldsymbol{l}}|\boldsymbol{w}, \boldsymbol{\theta}, \boldsymbol{y}) = \prod_{i=1}^n p(\tilde{l}_i|w_i, \boldsymbol{\theta}, \boldsymbol{y})$ , where  $\tilde{l}_i|\boldsymbol{\theta}, w_i, \boldsymbol{y}_i \sim N_+(A^{-1}B_i, A^{-1})$ , with  $A = 1 + \boldsymbol{\delta}^\top(\bar{\boldsymbol{\Omega}} - \boldsymbol{\delta}\boldsymbol{\delta}^\top)^{-1}\boldsymbol{\delta}$ ,  $B_i = w_i^{1/2}\boldsymbol{\delta}^\top(\bar{\boldsymbol{\Omega}} - \boldsymbol{\delta}\boldsymbol{\delta}^\top)^{-1}\boldsymbol{z}_i$  and  $N_+$  denotes a univariate normal distribution constrained to positive values. Similarly, at Step 2 the conditional posterior  $p(\boldsymbol{w}|\tilde{\boldsymbol{l}}, \boldsymbol{\theta}, \boldsymbol{y}) = \prod_{i=1}^n p(w_i|\tilde{l}_i, \boldsymbol{\theta}, \boldsymbol{y})$ , with

$$p(w_i|\boldsymbol{\theta}, \tilde{l}_i, \boldsymbol{y}) \propto w_i^{\frac{d+\nu}{2}-1} \exp\left\{-\frac{1}{2}\left(w_i\boldsymbol{z}_i^\top(\bar{\boldsymbol{\Omega}} - \boldsymbol{\delta}\boldsymbol{\delta}^\top)^{-1}\boldsymbol{z}_i - 2\tilde{l}_i w_i^{1/2}\boldsymbol{\delta}^\top(\bar{\boldsymbol{\Omega}} - \boldsymbol{\delta}\boldsymbol{\delta}^\top)^{-1}\boldsymbol{z}_i + w_i\nu\right)\right\}.$$

An adaptive random walk Metropolis-Hastings step is used to draw from this posterior.

In Step (b) of Algorithm 1, a draw of  $\tilde{\boldsymbol{l}}, \boldsymbol{w}$  is obtained by repeatedly drawing from the conditionals 25 times. We stress this is fast because all demanding computations do not involve  $\boldsymbol{l}$  and  $\boldsymbol{w}$ , so that they only need to be computed once per SGA step. We found 25 draws to be adequate, which is consistent with the findings in Loaiza-Maya et al. (2022) for other models.

## References

- Azzalini, A. and Capitanio, A. (2003). Distributions generated by perturbation of symmetry with emphasis on a multivariate skew t -distribution. *Journal of the Royal Statistical Society: Series B (Statistical Methodology)*, 65(2):367–389.
- Barndorff-Nielsen, O. (1977). Exponentially decreasing distributions for the logarithm of particle size. *Proceedings of the Royal Society of London. A. Mathematical and Physical Sciences*, 353(1674):401–419.
- Blei, D. M., Kucukelbir, A., and McAuliffe, J. D. (2017). Variational inference: A review for statisticians. *Journal of the American Statistical Association*, 112(518):859–877.
- Bollerslev, T. (1990). Modelling the coherence in short-run nominal exchange rates: A multivariate generalized arch model. *The Review of Economics and Statistics*, 72(3):498.
- Bollerslev, T., Patton, A. J., and Quaedvlieg, R. (2022). Realized semibetas: Disentangling “good” and “bad” downside risks. *Journal of Financial Economics*, 144(1):227–246.
- Bottou, L. (2010). Large-scale machine learning with stochastic gradient descent. In Lechevallier, Y. and Saporta, G., editors, *Proceedings of the 19th International Conference on Computational Statistics (COMPSTAT2010)*, pages 177–187. Springer.
- Britten-Jones, M. and Neuberger, A. (2000). Option prices, implied price processes, and stochastic volatility. *The journal of Finance*, 55(2):839–866.
- Chan, J. C. and Yu, X. (2022). Fast and accurate variational inference for large bayesian vars with stochastic volatility. *Journal of Economic Dynamics and Control*, 143:104505.
- Christoffersen, P., Errunza, V., Jacobs, K., and Langlois, H. (2012). Is the potential for international diversification disappearing? a dynamic copula approach. *Review of Financial Studies*, 25(12):3711–3751.
- Creal, D. D. and Tsay, R. S. (2015). High dimensional dynamic stochastic copula models. *Journal of Econometrics*, 189(2):335–345.
- Dattorro, J. (2005). *Convex Optimization & Euclidean Distance Geometry*. Meboo Publishing USA.
- Demarta, S. and Mcneil, A. J. (2005). The t copula and related copulas. *International Statistical Review*, 73(1):111–129.
- Engle, R. F. and Sokalska, M. E. (2012). Forecasting intraday volatility in the us equity market. multiplicative component garch. *Journal of Financial Econometrics*, 10(1):54–83.
- Fabozzi, F. J., Markowitz, H. M., and Gupta, F. (2008). Portfolio selection. *Handbook of finance*, 2.
- Gefang, D., Koop, G., and Poon, A. (2023). Forecasting using variational bayesian inference in large vector autoregressions with hierarchical shrinkage. *International Journal of Forecasting*, 39(1):346–363.
- Genton, M. G. (2004). *Skew-elliptical distributions and their applications: a journey beyond normality*. CRC Press.

- Geweke, J. (1991). Evaluating the accuracy of sampling-based approaches to the calculation of posterior moments. Staff Report 148, Federal Reserve Bank of Minneapolis.
- Giacometti, R., Torri, G., and Paterlini, S. (2021). Tail risks in large portfolio selection: penalized quantile and expectile minimum deviation models. *Quantitative Finance*, 21(2):243–261.
- Gneiting, T., Balabdaoui, F., and Raftery, A. E. (2007). Probabilistic forecasts, calibration and sharpness. *Journal of the Royal Statistical Society: Series B (Statistical Methodology)*, 69(2):243–268.
- Guidolin, M. and Timmermann, A. (2008). International asset allocation under regime switching, skew, and kurtosis preferences. *The Review of Financial Studies*, 21(2):889–935.
- Harvey, C. R., Liechty, J. C., Liechty, M. W., and Müller, P. (2010). Portfolio selection with higher moments. *Quantitative Finance*, 10(5):469–485.
- Hoffman, M. D., Gelman, A., et al. (2014). The no-u-turn sampler: adaptively setting path lengths in hamiltonian monte carlo. *J. Mach. Learn. Res.*, 15(1):1593–1623.
- Joe, H. (2014). *Dependence Modeling with Copulas*. Chapman and Hall/CRC.
- Kingma, D. P. and Welling, M. (2014). Auto-encoding variational bayes.
- Kollo, T. and Pettere, G. (2010). Parameter estimation and application of the multivariate skew t-copula. In *Copula theory and its applications*, pages 289–298. Springer.
- Krupskii, P. and Joe, H. (2013). Factor copula models for multivariate data. *Journal of Multivariate Analysis*, 120:85–101.
- Loaiza-Maya, R. and Nibbering, D. (2022). Fast variational bayes methods for multinomial probit models. *Journal of Business & Economic Statistics*, In Press(0):1–12.
- Loaiza-Maya, R. and Smith, M. S. (2019). Variational bayes estimation of discrete-margined copula models with application to time series. *Journal of Computational and Graphical Statistics*, 28(3):523–539.
- Loaiza-Maya, R., Smith, M. S., Nott, D. J., and Danaher, P. J. (2022). Fast and accurate variational inference for models with many latent variables. *Journal of Econometrics*, 230(2):339–362.
- Lucas, A., Schwaab, B., and Zhang, X. (2017). Modeling financial sector joint tail risk in the euro area. *Journal of Applied Econometrics*, 32(1):171–191.
- Markowitz, H. M. (1952). Portfolio selection. *The Journal of Finance*, 7.
- Miller, A. C., Foti, N. J., and Adams, R. P. (2017). Variational Boosting: Iteratively Refining Posterior Approximations. In Precup, D. and Teh, Y. W., editors, *Proceedings of the 34th International Conference on Machine Learning*, volume 70 of *Proceedings of Machine Learning Research*, pages 2420–2429. PMLR.
- Mishkin, A., Kunstner, F., Nielsen, D., Schmidt, M., and Khan, M. E. (2018). SLANG: Fast structured covariance approximations for Bayesian deep learning with natural gradient. *Advances in Neural Information Processing Systems*, 31.

- Murray, J. S., Dunson, D. B., Carin, L., and Lucas, J. E. (2013). Bayesian gaussian copula factor models for mixed data. *Journal of the American Statistical Association*, 108(502):656–665.
- Nelsen, R. B. (1999). *An Introduction to Copulas*. Springer.
- Nguyen, H., Ausín, M. C., and Galeano, P. (2020). Variational inference for high dimensional structured factor copulas. *Computational Statistics & Data Analysis*, 151:107012.
- Oh, D. H. and Patton, A. J. (2013). Simulated method of moments estimation for copula-based multivariate models. *Journal of the American Statistical Association*, 108(502):689–700.
- Oh, D. H. and Patton, A. J. (2017). Modeling dependence in high dimensions with factor copulas. *Journal of Business & Economic Statistics*, 35(1):139–154.
- Oh, D. H. and Patton, A. J. (2023). Dynamic factor copula models with estimated cluster assignments. *Journal of Econometrics*, In Press.
- Ong, V. M.-H., Nott, D. J., and Smith, M. S. (2018). Gaussian variational approximation with a factor covariance structure. *Journal of Computational and Graphical Statistics*, 27(3):465–478.
- Opschoor, A., Lucas, A., Barra, I., and Van Dijk, D. (2021). Closed-form multi-factor copula models with observation-driven dynamic factor loadings. *Journal of Business & Economic Statistics*, 39(4):1066–1079.
- Patton, A. J. (2006). Modelling asymmetric exchange rate dependence. *International Economic Review*, 47(2):527–556.
- Ranganath, R., Gerrish, S., and Blei, D. (2014). Black box variational inference. In *Artificial intelligence and statistics*, pages 814–822. PMLR.
- Sahu, S. K., Dey, D. K., and Branco, M. D. (2003). A new class of multivariate skew distributions with applications to bayesian regression models. *Canadian Journal of Statistics*, 31(2):129–150.
- Smith, M. S. (2021). Implicit Copulas: An Overview. *Econometrics and Statistics*, Forthcoming.
- Smith, M. S., Gan, Q., and Kohn, R. J. (2010). Modelling dependence using skew t copulas: Bayesian inference and applications. *Journal of Applied Econometrics*, 27(3):500–522.
- Smith, M. S. and Maneesoonthorn, W. (2018). Inversion copulas from nonlinear state space models with an application to inflation forecasting. *International Journal of Forecasting*, 34(3):389–407.
- Yoshida, T. (2018). Maximum likelihood estimation of skew-t copulas with its applications to stock returns. *Journal of Statistical Computation and Simulation*, 88(13):2489–2506.
- Zeiler, M. D. (2012). ADADELTA: An Adaptive Learning Rate Method. arXiv:1212.5701 [cs].
- Zhao, Z. (2021). Dynamic bivariate peak over threshold model for joint tail risk dynamics of financial markets. *Journal of Business & Economic Statistics*, 39(4):892–906.

# Online Appendix for “Efficient Variational Inference for Large Skew-t Copulas with Application to Intraday Equity Returns”

This Online Appendix has four parts:

**Part A:** Supporting information for Section 2.

**Part B:** Gradient for the AC skew-t copula with representation GR3.

**Part C:** Additional details for the simulation study in Section 4.

**Part D:** Additional details for Section 5.

## Appendix Part A Supporting Information for Section 2

### Part A.1 Density for the GH skew-t distribution

The joint density of  $\mathbf{Z}_{\text{GH}}$  is

$$f_{\mathbf{Z}_{\text{GH}}}(\mathbf{z}; \bar{\Omega}, \boldsymbol{\delta}, \nu) = \mathcal{A} \frac{K_{(\nu+d)/2} \left( \sqrt{(\nu + \mathbf{z}'\bar{\Omega}^{-1}\mathbf{z}) \boldsymbol{\delta}'\bar{\Omega}^{-1}\boldsymbol{\delta}} \right) \exp(\mathbf{z}'\bar{\Omega}^{-1}\boldsymbol{\delta})}{(\nu + \mathbf{z}'\bar{\Omega}^{-1}\mathbf{z}) \boldsymbol{\delta}'\bar{\Omega}^{-1}\boldsymbol{\delta})^{-\frac{\nu+d}{4}} \left( 1 + \frac{\mathbf{z}'\bar{\Omega}^{-1}\mathbf{z}}{\nu} \right)^{\frac{\nu+d}{2}}}, \text{ with}$$
$$\mathcal{A} = \frac{2^{\frac{2-\nu-d}{2}}}{\Gamma(\nu/2)(\pi\nu)^{d/2}|\bar{\Omega}|^{\frac{1}{2}}}.$$

The function  $K_{\beta}(s)$  is the modified Bessel function of the second kind with index  $\beta$ .

### Part A.2 Plot of the AC, SDB, G&H copula densities in Section 2

Figure A1 plots the bivariate copula model densities with  $N(0, 1)$  marginals and copula parameters which give the maximal asymmetric dependence at the 1% quantile (i.e. maximum value of  $\Delta(0, 1)$ .)

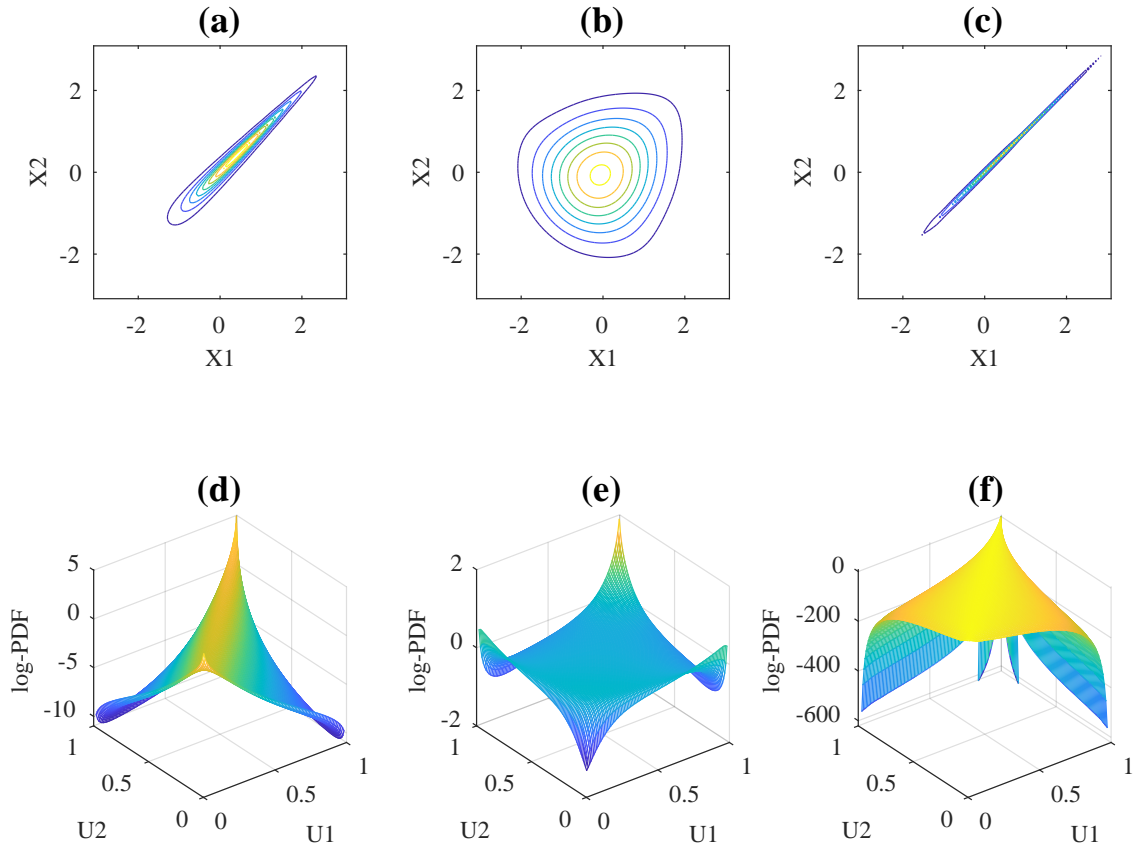


Figure A1: The first row plots density contours of three bivariate skew- $t$  copula models with  $N(0, 1)$  marginals and maximal asymmetric dependence  $\Delta(0.01)$  for (a) AC, (b) SDB, and (c) GH. The second row plots the logarithm of the corresponding copula densities.



## Appendix Part B Gradient for the AC skew-t copula with representation GR3

In this part of the Web Appendix we give further details on the VI methodology for the AC skew-t copula when using the generative representation GR3 with  $\boldsymbol{\psi} \equiv \{\boldsymbol{\theta}, \tilde{\boldsymbol{l}}, \boldsymbol{w}\}$ . We list the priors employed and then the log augmented posterior for this case. We derive the gradient  $\nabla_{\lambda} \log h(\boldsymbol{\psi})$  for this case, the result of which is given in Table 2 of the manuscript. This derivation uses the trace operator to express gradients as directional derivatives, which provides a computationally efficient expression.

### Part B.1 Priors

The parameters  $\boldsymbol{\theta} = \{\text{vech}(\tilde{G}), \boldsymbol{\delta}, \nu\}$  are transformed to unconstrained real values. Thus we defined  $\text{vech}(\tilde{G}) = \{G_{p,k}, \tilde{G}_{k,k}\}, p < k$ , to represent off-diagonal and diagonal values of  $\text{vech}(G)$  respectively,  $\tilde{G}_{k,k} = \log(\text{Diag}(G))$  denotes the logarithms of leading diagonal values in  $P \times K$  matrix  $G$  with  $K \ll P$ . And  $\tilde{\nu} = \log(\nu - 2)$  to promise VA inferenced  $\nu > 2$ .

The prior distribution is defined as  $p(\boldsymbol{\theta}) = p(G_{P,K})p(\tilde{G}_{K,K})p(\boldsymbol{\alpha})p(\tilde{\nu})$  with

$$\begin{aligned}
 (1) \quad p(G_{p,k}) &= f_{\text{GDP}}(G_{p,k}; a_1, b_1), p < k & (2) \quad p(\tilde{G}_{k,k}) &= f_{\text{GDP}}(\exp(\tilde{G}_{k,k}); a_1, b_1) \exp(\tilde{G}_{k,k}) \\
 (3) \quad p(\boldsymbol{\alpha}) &= \prod_{p=1}^P f_N(\alpha_p; 0, \sigma^2) & (4) \quad p(\tilde{\nu}) &= f_{\text{Gamma}}(\exp(\tilde{\nu}); a_2, b_2) \exp(\tilde{\nu})
 \end{aligned} \tag{A1}$$

### Part B.2 Log Posterior Representation

$$\begin{aligned}
 \log p(\boldsymbol{\theta}, \tilde{\boldsymbol{l}}, \boldsymbol{w} | \boldsymbol{y}) &= \left(\frac{d+v}{2} - 1\right) \sum_{i=1}^n \log(w_i) - \frac{n}{2} \log \left( \det \left( \bar{\Omega} - \boldsymbol{\delta} \boldsymbol{\delta}' \right) \right) \\
 &\quad + n \left( \frac{\nu}{2} \log \left( \frac{\nu}{2} \right) - \log \left( \Gamma \left( \frac{\nu}{2} \right) \right) \right) \\
 &\quad - \frac{1}{2} \sum_{i=1}^n \left\{ w_i \boldsymbol{y}'_i \left( \bar{\Omega} - \boldsymbol{\delta} \boldsymbol{\delta}' \right)^{-1} \boldsymbol{y}_i - 2 \tilde{l}_i w_i^{1/2} \boldsymbol{\delta}' \left( \bar{\Omega} - \boldsymbol{\delta} \boldsymbol{\delta}' \right)^{-1} \boldsymbol{y}_i \right. \\
 &\quad \left. + \tilde{l}_i^2 \boldsymbol{\delta}' \left( \bar{\Omega} - \boldsymbol{\delta} \boldsymbol{\delta}' \right)^{-1} \boldsymbol{\delta} + w_i \nu + \tilde{l}_i^2 w_i \right\} + \log p(\boldsymbol{\theta}) \\
 &= \mathcal{L}(\boldsymbol{y}, \tilde{\boldsymbol{l}}, \boldsymbol{w} | \boldsymbol{\theta}) + \log p(\boldsymbol{\theta})
 \end{aligned} \tag{A2}$$

, where  $\bar{\Omega} = V_1^{-1/2} V V_1^{-1/2}$ ,  $V = G G^\top + D$ ,  $V_1 = \text{diag}(V)^{-1/2}$  and  $\boldsymbol{\delta} = (1 + \boldsymbol{\alpha}^\top \bar{\Omega} \boldsymbol{\alpha})^{-1/2} \bar{\Omega} \boldsymbol{\alpha}$

**Part B.3** Computing  $\nabla_{G_{p,k}} \log p(\boldsymbol{\theta}, \tilde{\mathbf{l}}, \mathbf{w}|\mathbf{y})$ ,  $\nabla_{G_{k,k}} \log p(\boldsymbol{\theta}, \tilde{\mathbf{l}}, \mathbf{w}|\mathbf{y})$

$$\nabla_{G_{p,k}} \log p(\boldsymbol{\theta}, \tilde{\mathbf{l}}, \mathbf{w}|\mathbf{y}) = \nabla_{G_{p,k}} \left\{ \mathcal{L}(\mathbf{y}, \tilde{\mathbf{l}}, \mathbf{w}|\boldsymbol{\theta}) + \log p(G_{p,k}) \right\}, \quad \text{if } k < p,$$

$$\nabla_{\tilde{G}_{k,k}} \log p(\boldsymbol{\theta}, \tilde{\mathbf{l}}, \mathbf{w}|\mathbf{y}) = \nabla_{G_{k,k}} \left\{ \mathcal{L}(\mathbf{y}, \tilde{\mathbf{l}}, \mathbf{w}|\boldsymbol{\theta}) + \log p(G_{k,k}) \right\} \times \exp(\tilde{G}_{k,k}) + 1$$

$$\begin{aligned} \nabla_G \mathcal{L}(\mathbf{y}, \tilde{\mathbf{l}}, \mathbf{w}|\boldsymbol{\theta}) &= \nabla_G \left\{ -\frac{n}{2} \log \left( \det \left( \bar{\Omega} - \boldsymbol{\delta} \boldsymbol{\delta}' \right) \right) - \frac{1}{2} \sum_{i=1}^n \left( w_i \mathbf{y}'_i \left( \bar{\Omega} - \boldsymbol{\delta} \boldsymbol{\delta}' \right)^{-1} \mathbf{y}_i \right. \right. \\ &\quad \left. \left. - 2 \tilde{l}_i w_i^{1/2} \boldsymbol{\delta}' \left( \bar{\Omega} - \boldsymbol{\delta} \boldsymbol{\delta}' \right)^{-1} \mathbf{y}_i + \tilde{l}_i^2 \boldsymbol{\delta}' \left( \bar{\Omega} - \boldsymbol{\delta} \boldsymbol{\delta}' \right)^{-1} \boldsymbol{\delta} \right) \right\} \\ &= \nabla_G \left\{ -\frac{n}{2} T_{G1} - \frac{1}{2} \sum_{i=1}^n (T_{G2i} + T_{G3i} + T_{G4i}) \right\} \end{aligned} \quad (\text{A3})$$

with  $\boldsymbol{\delta} = (1 + \boldsymbol{\alpha}^\top \bar{\Omega} \boldsymbol{\alpha})^{-1/2} \bar{\Omega} \boldsymbol{\alpha}$  and  $\bar{\Omega} = V_1 V V_1$ ,  $V = G G^\top + D$ ,  $V_1 = \text{diag}(V)^{-1/2}$

**Part B.3.1** Computing  $\nabla_G T_{G1}$

$$T_{G1} = \log(\det(\bar{\Omega} - \boldsymbol{\delta} \boldsymbol{\delta}^\top)) \quad (\text{A4})$$

$$\begin{aligned} d T_{G1} &= d \log(\det(\bar{\Omega} - \boldsymbol{\delta} \boldsymbol{\delta}^\top)) \\ &= \text{tr}((\bar{\Omega} - \boldsymbol{\delta} \boldsymbol{\delta}^\top)^{-1} d(\bar{\Omega} - \boldsymbol{\delta} \boldsymbol{\delta}^\top)) \\ &= \text{tr}(C_0 d \bar{\Omega}) - \text{tr}(C_0 d(\boldsymbol{\delta} \boldsymbol{\delta}^\top)) \\ &= M_1 - M_2 \end{aligned} \quad (\text{A5})$$

By Woodbury formula and Sherman–Morrison formula, we have

$$\begin{aligned} \bar{\Omega} &= V_1 V V_1 \\ &= V_1 (G G^\top + D) V_1 \\ &= V_1 G G^\top V_1 + V_1 D V_1 \\ &= G_1 G_1^\top + D_1 \end{aligned} \quad (\text{A6})$$

$$\begin{aligned} \bar{\Omega}^{-1} &= (D_1 + G_1 G_1^\top)^{-1} \\ &= D_1^{-1} - D_1^{-1} G_1 (I_K + G_1^\top D_1^{-1} G_1)^{-1} G_1^\top D_1^{-1} \\ C_0 &= (\bar{\Omega} - \boldsymbol{\delta} \boldsymbol{\delta}^\top)^{-1} \\ &= \bar{\Omega}^{-1} + \frac{\bar{\Omega}^{-1} \boldsymbol{\delta} \boldsymbol{\delta}^\top \bar{\Omega}^{-1}}{1 - \boldsymbol{\delta}^\top \bar{\Omega}^{-1} \boldsymbol{\delta}} \end{aligned} \quad (\text{A7})$$

$$\begin{aligned}
M_1 &= \text{tr}(C_0 \text{d}\bar{\Omega}) \\
M_2 &= \text{tr}(C_0 \text{d}(\boldsymbol{\delta}\boldsymbol{\delta}^\top)) \\
&= \text{tr}\left(C_0 \text{d}((1 + \boldsymbol{\alpha}^\top \bar{\Omega} \boldsymbol{\alpha})^{-1} \bar{\Omega} \boldsymbol{\alpha} \boldsymbol{\alpha}^\top \bar{\Omega})\right) \\
&= \text{tr}\left(C_0 \text{d}(C_1^{-1} \bar{\Omega} \boldsymbol{\alpha} \boldsymbol{\alpha}^\top \bar{\Omega})\right) \\
&= \text{tr}\left(C_1^{-1} \boldsymbol{\alpha} \boldsymbol{\alpha}^\top \bar{\Omega} C_0 \text{d}\bar{\Omega}\right) + \text{tr}\left(C_1^{-1} C_0 \bar{\Omega} \boldsymbol{\alpha} \boldsymbol{\alpha}^\top \text{d}\bar{\Omega}\right) \\
&\quad + \text{tr}\left(-C_1^{-2} \boldsymbol{\alpha} \boldsymbol{\alpha}^\top \bar{\Omega} C_0 \bar{\Omega} \boldsymbol{\alpha} \boldsymbol{\alpha}^\top \text{d}\bar{\Omega}\right) \\
&= \text{tr}\left((C_1^{-1} C_2 C_0 + C_1^{-1} C_0 C_2^\top - C_1^{-2} C_2 C_0 C_2^\top) \text{d}\bar{\Omega}\right) \\
&= \text{tr}\left(C_3 \text{d}\bar{\Omega}\right)
\end{aligned} \tag{A8}$$

$$\begin{aligned}
M_1 - M_2 &= \text{tr}((C_0 - C_3) \text{d}\bar{\Omega}) \\
&= \text{tr}(C_4 \text{d}\bar{\Omega}) \\
&= \text{tr}(V V_1 C_4 \text{d}V_1) + \text{tr}(C_4 V_1 V \text{d}V_1) + \text{tr}(V_1 C_4 V_1 \text{d}V) \\
&= M_{1-1} + M_{1-2} + M_{1-3}
\end{aligned} \tag{A9}$$

where  $C_1 = 1 + \boldsymbol{\alpha}^\top \bar{\Omega} \boldsymbol{\alpha}$ ,  $C_2 = \boldsymbol{\alpha} \boldsymbol{\alpha}^\top \bar{\Omega}$ ,  $C_3 = C_1^{-1} C_2 C_0 + C_1^{-1} C_0 C_2^\top - C_1^{-2} C_2 C_0 C_2^\top$ ,  $C_4 = C_0 - C_3$

$$\begin{aligned}
M_{1-1} &= \text{tr}(V V_1 C_4 \text{d}V_1) \\
&= \text{tr}\left(-\frac{1}{2} V^{-3/2} \odot (V V_1 C_4) \text{d}V\right) \\
&= \text{tr}\left(-\frac{1}{2} G^\top (V_2 \odot (V V_1 C_4)) \text{d}G\right) \\
&\quad + \text{tr}\left(-\frac{1}{2} (V_2 \odot (V V_1 C_4)) G \text{d}G^\top\right) \\
&= \text{tr}\left(-\frac{1}{2} (V_2 \odot (V V_1 C_4 + (V V_1 C_4)^\top)) G \text{d}G^\top\right)
\end{aligned} \tag{A10}$$

$$\begin{aligned}
M_{1-2} &= \text{tr}(C_4 V_1 V \text{d}V_1) \\
&= \text{tr}\left(-\frac{1}{2} (V_2 \odot (C_4 V_1 V + (C_4 V_1 V)^\top)) G \text{d}G^\top\right)
\end{aligned} \tag{A11}$$

$$\begin{aligned}
M_{1-3} &= \text{tr}(V_1 C_4 V_1 \text{d}V) \\
&= \text{tr}(V_1 C_4 V_1 \text{d}G G^\top) \\
&= \text{tr}(G^\top V_1 C_4 V_1 \text{d}G) + \text{tr}(V_1 C_4 V_1 G \text{d}G^\top) \\
&= \text{tr}((V_1 C_4 V_1 + (V_1 C_4 V_1)^\top) G \text{d}G^\top)
\end{aligned} \tag{A12}$$

, where  $V_2 = \text{diag}(V)^{-3/2}$ .

From above we could derive the gradient of  $T_{G1}$

$$\nabla_G T_{G1} = -2(V_2 \odot V V_1 C_4 + V_1 C_4 V_1) G \tag{A13}$$

**Part B.3.2**  $\nabla_G T_{G2i}$

$$T_{G2i} = w_i \mathbf{y}_i^\top (\bar{\Omega} - \boldsymbol{\delta} \boldsymbol{\delta}^\top)^{-1} \mathbf{y}_i \quad (\text{A14})$$

$$\begin{aligned} dT_{G2i} &= \text{tr} \left( -w_i (\bar{\Omega} - \boldsymbol{\delta} \boldsymbol{\delta}^\top)^{-1} \mathbf{y}_i \mathbf{y}_i^\top (\bar{\Omega} - \boldsymbol{\delta} \boldsymbol{\delta}^\top)^{-1} d(\bar{\Omega} - \boldsymbol{\delta} \boldsymbol{\delta}^\top) \right) \\ &= \text{tr} \left( C_{5i} d\bar{\Omega} \right) - \text{tr} \left( C_{5i} d\boldsymbol{\delta} \boldsymbol{\delta}^\top \right) \\ &= M_3 - M_4 \end{aligned} \quad (\text{A15})$$

where  $C_{5i} = -w_i (\bar{\Omega} - \boldsymbol{\delta} \boldsymbol{\delta}^\top)^{-1} \mathbf{y}_i \mathbf{y}_i^\top (\bar{\Omega} - \boldsymbol{\delta} \boldsymbol{\delta}^\top)^{-1} = -w_i C_0 \mathbf{y}_i \mathbf{y}_i^\top C_0$

$$\begin{aligned} M_3 &= \text{tr}(C_{5i} d\bar{\Omega}) \\ M_4 &= \text{tr} \left( C_{5i} d\boldsymbol{\delta} \boldsymbol{\delta}^\top \right) \\ &= \text{tr} \left( C_1^{-1} C_2 C_{5i} + C_1^{-1} C_{5i} C_2^\top - C_1^{-2} C_2 C_{5i} C_2^\top d\bar{\Omega} \right) \\ &= \text{tr}(C_{6i} d\bar{\Omega}) \end{aligned} \quad (\text{A16})$$

$$\begin{aligned} M_3 - M_4 &= \text{tr}((C_{5i} - C_{6i}) d\bar{\Omega}) \\ &= \text{tr}(C_{7i} d\bar{\Omega}) \end{aligned} \quad (\text{A17})$$

where  $C_{6i} = C_1^{-1} C_2 C_{5i} + C_1^{-1} C_{5i} C_2^\top - C_1^{-2} C_2 C_{5i} C_2^\top$ ,  $C_{7i} = C_{5i} - C_{6i}$

From above we could derive the gradient of  $T_{G2i}$

$$\nabla_G T_{G2i} = -2(V_2 \odot V V_1 C_{7i} + V_1 C_{7i} V_1) G \quad (\text{A18})$$

**Part B.3.3** **Computing**  $\nabla_G T_{G3i}$

$$T_{G3i} = -2\tilde{l}_i w_i^{1/2} \boldsymbol{\delta}^\top (\bar{\Omega} - \boldsymbol{\delta} \boldsymbol{\delta}^\top)^{-1} \mathbf{y}_i \quad (\text{A19})$$

$$\begin{aligned} dT_{G3i} &= \text{tr} \left( -2\tilde{l}_i w_i^{1/2} (\bar{\Omega} - \boldsymbol{\delta} \boldsymbol{\delta}^\top)^{-1} \mathbf{y}_i d\boldsymbol{\delta}^\top \right) + \text{tr} \left( -2\tilde{l}_i w_i^{1/2} \mathbf{y}_i \boldsymbol{\delta}^\top d(\bar{\Omega} - \boldsymbol{\delta} \boldsymbol{\delta}^\top)^{-1} \right) \\ &= \text{tr} \left( -2\tilde{l}_i w_i^{1/2} (1 + \boldsymbol{\alpha}^\top \bar{\Omega} \boldsymbol{\alpha})^{-1/2} (\bar{\Omega} - \boldsymbol{\delta} \boldsymbol{\delta}^\top)^{-1} \mathbf{y}_i \boldsymbol{\alpha}^\top d\bar{\Omega} \right) \\ &\quad + \text{tr} \left( \tilde{l}_i w_i^{1/2} (1 + \boldsymbol{\alpha}^\top \bar{\Omega} \boldsymbol{\alpha})^{-3/2} \boldsymbol{\alpha} \boldsymbol{\alpha}^\top \bar{\Omega} (\bar{\Omega} - \boldsymbol{\delta} \boldsymbol{\delta}^\top)^{-1} \mathbf{y}_i \boldsymbol{\alpha}^\top d\bar{\Omega} \right) \\ &\quad + \text{tr} \left( 2\tilde{l}_i w_i^{1/2} (\bar{\Omega} - \boldsymbol{\delta} \boldsymbol{\delta}^\top)^{-1} \mathbf{y}_i \boldsymbol{\delta}^\top (\bar{\Omega} - \boldsymbol{\delta} \boldsymbol{\delta}^\top)^{-1} d\bar{\Omega} \right) \\ &\quad - \text{tr} \left( 2\tilde{l}_i w_i^{1/2} (\bar{\Omega} - \boldsymbol{\delta} \boldsymbol{\delta}^\top)^{-1} \mathbf{y}_i \boldsymbol{\delta}^\top (\bar{\Omega} - \boldsymbol{\delta} \boldsymbol{\delta}^\top)^{-1} d\boldsymbol{\delta} \boldsymbol{\delta}^\top \right) \\ &= \text{tr}((C_{8i} + C_{9i}) d\bar{\Omega}) - \text{tr}(C_{9i} d\boldsymbol{\delta} \boldsymbol{\delta}^\top) \\ &= M_5 - M_6 \end{aligned} \quad (\text{A20})$$

where  $C_{8i} = -2\tilde{l}_i w_i^{1/2} C_1^{-1/2} C_0 \mathbf{y}_i \boldsymbol{\alpha}^\top + \tilde{l}_i w_i^{1/2} C_1^{-3/2} C_2 C_0 \mathbf{y}_i \boldsymbol{\alpha}^\top$ ,  $C_{9i} = 2\tilde{l}_i w_i^{1/2} C_0 \mathbf{y}_i \boldsymbol{\delta}^\top C_0$ .

$$\begin{aligned}
M_5 &= \text{tr}((C_{8i} + C_{9i}) \text{d}\bar{\Omega}) \\
M_6 &= \text{tr}(C_{9i} \text{d}\boldsymbol{\delta} \boldsymbol{\delta}^\top) \\
&= \text{tr}\left((C_1^{-1} C_2 C_{9i} + C_1^{-1} C_{9i} C_2^\top - C_1^{-2} C_2 C_{9i} C_2^\top) \text{d}\bar{\Omega}\right) \\
&= \text{tr}(C_{10i} \text{d}\bar{\Omega})
\end{aligned} \tag{A21}$$

$$\begin{aligned}
M_5 - M_6 &= \text{tr}((C_{8i} + C_{9i} - C_{10i}) \text{d}\bar{\Omega}) \\
&= \text{tr}(C_{11i} \text{d}\bar{\Omega})
\end{aligned} \tag{A22}$$

where  $C_{10i} = C_1^{-1} C_2 C_{9i} + C_1^{-1} C_{9i} C_2^\top - C_1^{-2} C_2 C_{9i} C_2^\top$ ,  $C_{11i} = C_{8i} + C_{9i} - C_{10i}$

$$\nabla_G T_{G3i} = -2(V_2 \odot V V_1 C_{11i} + V_1 C_{11i} V_1) G \tag{A23}$$

### Part B.3.4 Computing $\nabla_G T_{G4i}$

$$T_{G4i} = \tilde{l}_i^2 \boldsymbol{\delta}^\top (\bar{\Omega} - \boldsymbol{\delta} \boldsymbol{\delta}^\top)^{-1} \boldsymbol{\delta} \tag{A24}$$

$$\begin{aligned}
\text{d}T_{G4i} &= \text{tr}\left(2\tilde{l}_i^2 (\bar{\Omega} - \boldsymbol{\delta} \boldsymbol{\delta}^\top)^{-1} \boldsymbol{\delta} \text{d}\boldsymbol{\delta}^\top\right) + \text{tr}\left(\tilde{l}_i^2 \boldsymbol{\delta} \boldsymbol{\delta}^\top \text{d}(\bar{\Omega} - \boldsymbol{\delta} \boldsymbol{\delta}^\top)^{-1}\right) \\
&= \text{tr}\left(\tilde{l}_i^2 C_1^{(-1/2)} C_0 \boldsymbol{\delta} \boldsymbol{\alpha}^\top \text{d}\bar{\Omega}\right) + \text{tr}\left(-\frac{1}{2} \tilde{l}_i^2 C_1^{-3/2} \boldsymbol{\alpha} \boldsymbol{\alpha}^\top \bar{\Omega} C_0 \boldsymbol{\delta} \boldsymbol{\alpha}^\top \text{d}\bar{\Omega}\right) \\
&+ \text{tr}\left(-\tilde{l}_i^2 C_0 \boldsymbol{\delta} \boldsymbol{\delta}^\top C_0 \text{d}\bar{\Omega}\right) - \text{tr}\left(-\tilde{l}_i^2 C_0 \boldsymbol{\delta} C_0 \text{d}\boldsymbol{\delta} \boldsymbol{\delta}^\top\right) \\
&= \text{tr}((C_{12i} + C_{13i}) \text{d}\bar{\Omega}) - \text{tr}(C_{13i} \text{d}\boldsymbol{\delta} \boldsymbol{\delta}^\top) \\
&= M_7 - M_8
\end{aligned} \tag{A25}$$

where  $C_{12i} = 2\tilde{l}_i^2 C_1^{(-1/2)} \boldsymbol{\alpha} \boldsymbol{\delta}^\top C_0 - \tilde{l}_i^2 C_1^{-3/2} \boldsymbol{\alpha} \boldsymbol{\delta}^\top C_0 C_2^\top$ ,  $C_{13i} = -\tilde{l}_i^2 C_0 \boldsymbol{\delta} \boldsymbol{\delta}^\top C_0$ .

$$\begin{aligned}
M_7 &= \text{tr}((C_{12i} + C_{13i}) \text{d}\bar{\Omega}) \\
M_8 &= \text{tr}(C_{13i} \text{d}\boldsymbol{\delta} \boldsymbol{\delta}^\top) \\
&= \text{tr}\left((C_1^{-1} C_2 C_{13i} + C_1^{-1} C_{13i} C_2^\top - C_1^{-2} C_2 C_{13i} C_2^\top) \text{d}\bar{\Omega}\right) \\
&= \text{tr}(C_{14i} \text{d}\bar{\Omega})
\end{aligned} \tag{A26}$$

$$\begin{aligned}
M_7 - M_8 &= \text{tr}((C_{12i} + C_{13i} - C_{14i}) \text{d}\bar{\Omega}) \\
&= \text{tr}(C_{15i} \text{d}\bar{\Omega})
\end{aligned} \tag{A27}$$

where  $C_{14i} = C_1^{-1} C_2 C_{13i} + C_1^{-1} C_{13i} C_2^\top - C_1^{-2} C_2 C_{13i} C_2^\top$ ,  $C_{15i} = C_{12i} + C_{13i} - C_{14i}$

$$\nabla_G T_{G4i} = -2(V_2 \odot V V_1 C_{15i} + V_1 C_{15i} V_1) G \quad (\text{A28})$$

**Part B.3.5 Computing  $\nabla_{G_{p,k}} \log p(G_{p,k})$**

$$\begin{aligned} \frac{\partial}{\partial G_{p,k}} \log(p(G)) &= \frac{\partial}{\partial G_{p,k}} \log(f_{\text{GDP}}(G_{p,k}, a_1, b_1)) \\ &= \frac{\partial}{\partial G_{p,k}} \left( - (a_1 + 1) \log\left(1 + \frac{|G_{p,k}|}{b_1}\right) \right) \\ &= -(a_1 + 1) \text{sign}(G_{p,k}) \frac{1}{b_1 + |G_{p,k}|} \end{aligned} \quad (\text{A29})$$

**Part B.4 Computing  $\nabla_{\alpha} \log p(\theta, \tilde{l}, \mathbf{w} | \mathbf{y})$**

$$\begin{aligned} \nabla_{\alpha} \mathcal{L}(\mathbf{y}, \tilde{l}, \mathbf{w} | \theta) &= \nabla_{\alpha} \left( -\frac{n}{2} \log \left( \det(\bar{\Omega} - \delta \delta^{\top}) \right) \right. \\ &\quad \left. - \frac{1}{2} \sum_{i=1}^n \left( w_i \mathbf{y}_i^{\top} (\bar{\Omega} - \delta \delta^{\top})^{-1} \mathbf{y}_i - 2 \tilde{l}_i w_i^{1/2} \delta^{\top} (\bar{\Omega} - \delta \delta^{\top})^{-1} \mathbf{y}_i \right. \right. \\ &\quad \left. \left. + \tilde{l}_i^2 \delta^{\top} (\bar{\Omega} - \delta \delta^{\top})^{-1} \delta \right) \right) \\ &= \nabla_{\alpha} \left( -\frac{n}{2} T_{\alpha 1} - \frac{1}{2} \sum_{i=1}^n (T_{\alpha 2i} + T_{\alpha 3i} + T_{\alpha 4i}) \right) \end{aligned} \quad (\text{A30})$$

**Part B.4.1 Computing  $\nabla_{\alpha} T_{\alpha 1}$**

$$T_{\alpha 1} = \log(\det(\bar{\Omega} - \delta \delta^{\top})) \quad (\text{A31})$$

$$\begin{aligned} d T_{\alpha 1} &= \text{tr}((\bar{\Omega} - \delta \delta^{\top})^{-1} d(\bar{\Omega} - \delta \delta^{\top})) \\ &= \text{tr}(-C_0 d(\delta \delta^{\top})) \\ &= \text{tr}(-2C_0 \delta d \delta^{\top}) \\ &= \text{tr}(-2C_0 \delta d(1 + \alpha^{\top} \bar{\Omega} \alpha)^{(-1/2)} \alpha^{\top} \bar{\Omega}) \\ &= \text{tr}(-2C_1^{-1/2} \bar{\Omega} C_0 \delta d \alpha^{\top} + C_1^{-3/2} \bar{\Omega} \alpha (\alpha^{\top} \bar{\Omega} C_0 \delta) d \alpha^{\top} + C_1^{-3/2} (\alpha^{\top} \bar{\Omega} C_0 \delta) \alpha^{\top} \bar{\Omega} d \alpha) \\ &= \text{tr}(-2C_1^{-1/2} \bar{\Omega} C_0 \delta d \alpha^{\top} + 2C_1^{-3/2} \bar{\Omega} \alpha (\alpha^{\top} \bar{\Omega} C_0 \delta) d \alpha^{\top}) \end{aligned} \quad (\text{A32})$$

$$\nabla_{\alpha} T_{\alpha 1} = 2C_1^{-3/2} \bar{\Omega} \alpha (\alpha^{\top} \bar{\Omega} C_0 \delta) - 2C_1^{-1/2} \bar{\Omega} C_0 \delta \quad (\text{A33})$$

**Part B.4.2 Computing  $\nabla_{\alpha} T_{\alpha 2i}$**

$$T_{\alpha 2i} = w_i \mathbf{y}_i^{\top} (\bar{\Omega} - \delta \delta^{\top})^{-1} \mathbf{y}_i \quad (\text{A34})$$

$$\begin{aligned} d T_{\alpha 2i} &= \text{tr}(w_i \mathbf{y}_i^{\top} d(\bar{\Omega} - \delta \delta^{\top})^{-1} \mathbf{y}_i) \\ &= \text{tr}(-w_i C_0 \mathbf{y}_i \mathbf{y}_i^{\top} C_0 d(\bar{\Omega} - \delta \delta^{\top})) \\ &= \text{tr}(w_i C_0 \mathbf{y}_i \mathbf{y}_i^{\top} C_0 d(\delta \delta^{\top})) \\ &= \text{tr}(2w_i C_0 \mathbf{y}_i \mathbf{y}_i^{\top} C_0 \delta d \delta^{\top}) \\ &= \text{tr}(2C_{5i} \delta d(1 + \alpha^{\top} \bar{\Omega} \alpha)^{-1/2} \alpha^{\top} \bar{\Omega}) \\ &= \text{tr}(2C_1^{-1/2} \bar{\Omega} C_{5i} \delta d \alpha^{\top}) + \text{tr}(-C_1^{-3/2} C_{5i} \bar{\Omega} \alpha \alpha^{\top} \bar{\Omega} d \alpha) + \text{tr}(-C_1^{-3/2} \bar{\Omega} \alpha C_{5i} \bar{\Omega} \alpha d \alpha^{\top}) \end{aligned} \quad (\text{A35})$$

$$\nabla_{\alpha} T_{\alpha 2i} = C_1^{-2} \bar{\Omega} \alpha \alpha^{\top} \bar{\Omega} (C_{5i} + C_{5i}^{\top}) \bar{\Omega} \alpha - C_1^{-1} \bar{\Omega} (C_{5i} + C_{5i}^{\top}) \bar{\Omega} \alpha \quad (\text{A36})$$

**Part B.4.3 Computing  $\nabla_{\alpha} T_{\alpha 3i}$**

$$T_{\alpha 3i} = -2\tilde{l}_i w_i^{1/2} \delta^{\top} (\bar{\Omega} - \delta \delta^{\top})^{-1} \mathbf{y}_i \quad (\text{A37})$$

$$\begin{aligned} d T_{\alpha 3i} &= \text{tr}(-2\tilde{l}_i w_i^{1/2} (\bar{\Omega} - \delta \delta^{\top})^{-1} \mathbf{y}_i d \delta^{\top}) \\ &\quad + \text{tr}(2\tilde{l}_i w_i^{1/2} (\bar{\Omega} - \delta \delta^{\top})^{-1} \mathbf{y}_i \delta^{\top} (\bar{\Omega} - \delta \delta^{\top})^{-1} d(\bar{\Omega} - \delta \delta^{\top})) \\ &= M_9 + M_{10} \\ M_9 &= \text{tr}(-2\tilde{l}_i w_i^{1/2} (\bar{\Omega} - \delta \delta^{\top})^{-1} \mathbf{y}_i d((1 + \alpha^{\top} \bar{\Omega} \alpha)^{-1/2} \alpha^{\top} \bar{\Omega})) \\ &= \text{tr}(-2\tilde{l}_i w_i^{1/2} C_1^{-1/2} \bar{\Omega} C_0 \mathbf{y}_i d \alpha^{\top}) + \text{tr}(\tilde{l}_i w_i^{1/2} C_1^{-3/2} \bar{\Omega} \alpha \alpha^{\top} \bar{\Omega} C_0 \mathbf{y}_i d \alpha^{\top}) \\ &\quad + \text{tr}(\tilde{l}_i w_i^{1/2} C_1^{-3/2} \alpha^{\top} \bar{\Omega} C_0 \mathbf{y}_i \alpha^{\top} \bar{\Omega} d \alpha) \\ &= \text{tr}(C_{16i} d \alpha^{\top}) \\ M_{10} &= \text{tr}(2\tilde{l}_i w_i^{1/2} (\bar{\Omega} - \delta \delta^{\top})^{-1} \mathbf{y}_i \delta^{\top} (\bar{\Omega} - \delta \delta^{\top})^{-1} d(\bar{\Omega} - \delta \delta^{\top})) \\ &= \text{tr}(-2\tilde{l}_i w_i^{1/2} (\bar{\Omega} - \delta \delta^{\top})^{-1} \mathbf{y}_i \delta^{\top} (\bar{\Omega} - \delta \delta^{\top})^{-1} d(\delta \delta^{\top})) \\ &= \text{tr}(C_{17i} d((1 + \alpha^{\top} \bar{\Omega} \alpha)^{-1} \bar{\Omega} \alpha \alpha^{\top} \bar{\Omega})) \\ &= \text{tr}(C_1^{-1} \alpha^{\top} \bar{\Omega} C_{17i} \bar{\Omega} d \alpha) + \text{tr}(C_1^{-1} \bar{\Omega} C_{17i} \bar{\Omega} \alpha d \alpha^{\top}) \\ &\quad + \text{tr}(-C_1^{-2} \bar{\Omega} \alpha \alpha^{\top} \bar{\Omega} C_{17i} \bar{\Omega} \alpha d \alpha^{\top}) + \text{tr}(-C_1^{-2} \alpha^{\top} \bar{\Omega} C_{17i} \bar{\Omega} \alpha \alpha^{\top} \bar{\Omega} d \alpha) \end{aligned} \quad (\text{A38})$$

where  $C_{16i} = -2\tilde{l}_i w_i^{1/2} C_1^{-1/2} \bar{\Omega} C_0 \mathbf{y}_i + 2\tilde{l}_i w_i^{1/2} C_1^{-3/2} \alpha^{\top} \bar{\Omega} C_0 \mathbf{y}_i \bar{\Omega} \alpha$ ,  $C_{17i} = -2\tilde{l}_i w_i^{1/2} C_0 \mathbf{y}_i \delta^{\top} C_0$

$$\nabla_{\alpha} T_{\alpha 3i} = C_{16i} + C_1^{-1} \bar{\Omega} (C_{17i} + C_{17i}^{\top}) \bar{\Omega} \alpha - C_1^{-2} \bar{\Omega} \alpha \alpha^{\top} \bar{\Omega} (C_{17i} + C_{17i}^{\top}) \bar{\Omega} \alpha \quad (\text{A39})$$

**Part B.4.4 Computing  $\nabla_{\alpha} T_{\alpha 4}$**

$$T_{\alpha 4} = \tilde{l}_i^2 \boldsymbol{\delta}^{\top} (\bar{\Omega} - \boldsymbol{\delta} \boldsymbol{\delta}^{\top})^{-1} \boldsymbol{\delta} \quad (\text{A40})$$

$$\begin{aligned} dT_{\alpha 4} &= \text{tr}(\tilde{l}_i^2 (\bar{\Omega} - \boldsymbol{\delta} \boldsymbol{\delta}^{\top})^{-1} \boldsymbol{\delta} d\boldsymbol{\delta}^{\top}) + \text{tr}(\tilde{l}_i^2 \boldsymbol{\delta}^{\top} (\bar{\Omega} - \boldsymbol{\delta} \boldsymbol{\delta}^{\top})^{-1} d\boldsymbol{\delta}) \\ &\quad + \text{tr}(-\tilde{l}_i^2 (\bar{\Omega} - \boldsymbol{\delta} \boldsymbol{\delta}^{\top})^{-1} \boldsymbol{\delta} \boldsymbol{\delta}^{\top} (\bar{\Omega} - \boldsymbol{\delta} \boldsymbol{\delta}^{\top})^{-1} d(\bar{\Omega} - \boldsymbol{\delta} \boldsymbol{\delta}^{\top})) \\ &= 2M_{11} + M_{12} \end{aligned} \quad (\text{A41})$$

$$\begin{aligned} M_{11} &= \text{tr}(\tilde{l}_i^2 (\bar{\Omega} - \boldsymbol{\delta} \boldsymbol{\delta}^{\top})^{-1} \boldsymbol{\delta} d\boldsymbol{\delta}^{\top}) \\ &= \text{tr}(\tilde{l}_i^2 C_0 \boldsymbol{\delta} d((1 + \boldsymbol{\alpha}^{\top} \bar{\Omega} \boldsymbol{\alpha})^{(-1/2)} \boldsymbol{\alpha}^{\top} \bar{\Omega})) \\ &= \text{tr}(\tilde{l}_i^2 C_1^{-1/2} \bar{\Omega} C_0 \boldsymbol{\delta} d\boldsymbol{\alpha}^{\top}) \\ &\quad + \text{tr}(-\frac{1}{2} \tilde{l}_i^2 C_1^{-3/2} \bar{\Omega} \boldsymbol{\alpha} \boldsymbol{\alpha}^{\top} \bar{\Omega} C_0 \boldsymbol{\delta} d\boldsymbol{\alpha}^{\top}) + \text{tr}(-\frac{1}{2} \tilde{l}_i^2 C_1^{-3/2} \boldsymbol{\alpha}^{\top} \bar{\Omega} C_0 \boldsymbol{\delta} \boldsymbol{\alpha}^{\top} \bar{\Omega} d\boldsymbol{\alpha}) \\ &= \text{tr}(C_{18i} d\boldsymbol{\alpha}^{\top}) \end{aligned} \quad (\text{A42})$$

$$\begin{aligned} M_{12} &= \text{tr}(\tilde{l}_i^2 C_0 \boldsymbol{\delta} \boldsymbol{\delta}^{\top} C_0 d(\boldsymbol{\delta} \boldsymbol{\delta}^{\top})) \\ &= \text{tr}(C_{19i} d((1 + \boldsymbol{\alpha}^{\top} \bar{\Omega} \boldsymbol{\alpha})^{-1} \bar{\Omega} \boldsymbol{\alpha} \boldsymbol{\alpha}^{\top} \bar{\Omega})) \\ &= \left( \text{tr}(C_1^{-1} \boldsymbol{\alpha}^{\top} \bar{\Omega} C_{19i} \bar{\Omega} d\boldsymbol{\alpha}) + \text{tr}(C_1^{-1} \bar{\Omega} C_{19i} \bar{\Omega} \boldsymbol{\alpha} d\boldsymbol{\alpha}^{\top}) \right. \\ &\quad \left. + \text{tr}(-C_1^{-2} \bar{\Omega} \boldsymbol{\alpha} \boldsymbol{\alpha}^{\top} \bar{\Omega} C_{19i} \bar{\Omega} \boldsymbol{\alpha} d\boldsymbol{\alpha}^{\top}) + \text{tr}(-C_1^{-2} \boldsymbol{\alpha}^{\top} \bar{\Omega} C_{19i} \bar{\Omega} \boldsymbol{\alpha} \boldsymbol{\alpha}^{\top} \bar{\Omega} d\boldsymbol{\alpha}) \right) \end{aligned}$$

where  $C_{18i} = \tilde{l}_i^2 C_1^{-1/2} \bar{\Omega} C_0 \boldsymbol{\delta} - \tilde{l}_i^2 C_1^{-3/2} \bar{\Omega} \boldsymbol{\alpha} \boldsymbol{\alpha}^{\top} \bar{\Omega} C_0 \boldsymbol{\delta}$ ,  $C_{19i} = \tilde{l}_i^2 C_0 \boldsymbol{\delta} \boldsymbol{\delta}^{\top} C_0$

$$\nabla_{\alpha} T_{\alpha 4i} = 2C_{18i} + C_1^{-1} \bar{\Omega} (C_{19i} + C_{19i}^{\top}) \bar{\Omega} \boldsymbol{\alpha} - C_1^{-2} \bar{\Omega} \boldsymbol{\alpha} \boldsymbol{\alpha}^{\top} \bar{\Omega} (C_{19i} + C_{19i}^{\top}) \bar{\Omega} \boldsymbol{\alpha} \quad (\text{A43})$$

**Part B.4.5 Computing  $\nabla_{\alpha} \log p(\boldsymbol{\alpha})$**

$$\begin{aligned} \nabla_{\alpha_i} \log p(\alpha_i) &\propto \nabla_{\alpha_i} \left( -\frac{1}{2\sigma^2} \alpha_i^2 \right) \\ &\propto -\frac{1}{\sigma^2} \alpha_i \end{aligned} \quad (\text{A44})$$



**Part B.5** Computing  $\nabla_{\tilde{\nu}} \log p(\boldsymbol{\theta}, \tilde{\mathbf{l}}, \mathbf{w}|\mathbf{y})$

$$\begin{aligned}
\nabla_{\tilde{\nu}} \log g(x, \boldsymbol{\theta}, L) &= \nabla_{\tilde{\nu}} \left\{ \mathcal{L}(\mathbf{y}, \tilde{\mathbf{l}}, \mathbf{w}|\boldsymbol{\theta}) + \log(p(\nu)) + \log\left(\frac{d\nu}{d\tilde{\nu}}\right) \right\} \\
&= \nabla_{\tilde{\nu}} \left\{ \mathcal{L}(\mathbf{y}, \tilde{\mathbf{l}}, \mathbf{w}|\boldsymbol{\theta}) + \log(p(\nu)) + \tilde{\nu} + \log(2) \right\} \\
&= \nabla_{\nu} \left\{ \mathcal{L}(\mathbf{y}, \tilde{\mathbf{l}}, \mathbf{w}|\boldsymbol{\theta}) + \log(p(\nu)) \right\} \frac{d\nu}{d\tilde{\nu}} + \frac{d}{d\tilde{\nu}} (\tilde{\nu} + \log(2)) \\
&= \nabla_{\nu} \left\{ \mathcal{L}(\mathbf{y}, \tilde{\mathbf{l}}, \mathbf{w}|\boldsymbol{\theta}) + \log(p(\nu)) \right\} \times \exp(\tilde{\nu}) + 1
\end{aligned} \tag{A45}$$

$$\begin{aligned}
\nabla_{\nu} \mathcal{L}(\mathbf{y}, \tilde{\mathbf{l}}, \mathbf{w}|\boldsymbol{\theta}) &= \nabla_{\nu} \left\{ \frac{\nu}{2} \sum_{i=1}^n \log(w_i) + n \left( \frac{\nu}{2} \log\left(\frac{\nu}{2}\right) - \log\left(\Gamma\left(\frac{\nu}{2}\right)\right) \right) - \frac{1}{2} \sum_{i=1}^n w_i \nu \right\} \\
&= \frac{1}{2} \sum_{i=1}^n \log(w_i) + n \left( \frac{1}{2} \log\left(\frac{\nu}{2}\right) + \frac{1}{2} - \frac{1}{2} \psi_0\left(\frac{\nu}{2}\right) \right) - \frac{1}{2} \sum_{i=1}^n w_i
\end{aligned} \tag{A46}$$

, where  $\psi_0(t) = \frac{d \log(\Gamma(t))}{d(t)}$  is the digamma function

$$\begin{aligned}
\nabla_{\nu} \log(p(\nu)) &= \nabla_{\nu} \log \left( f_{Gamma}(\nu, a_2, b_2) \right) \\
&= \nabla_{\nu} \left( (a_2 - 1) \log(\nu) - b_2 \nu \right) \\
&= (a_2 - 1) \frac{1}{\nu} - b_2
\end{aligned} \tag{A47}$$

## Appendix Part C Additional Details for the Simulation

This web appendix provides additional details for the simulation in Section 4.

### Part C.1 DGPs

In Case 1 the dimension  $d = 5$  and number of factors  $k = 1$ , with parameters obtained by fitting the skew-t copula with  $\nu = 10$  to  $n = 1040$  observations of 15 minute returns in the period between 2019-Sep-11 and 2019-Nov-6. The parameter values are:

$$\begin{aligned}\alpha &= [6.7933, -0.6313, -0.0269, 0.2665, -1.0225]^\top \\ G &= [0.7526, 0.6048, 3.1338, 2.5151, 0.7016]^\top \\ \nu &= 10\end{aligned}$$

In Case 2 the dimension  $d = 30$  and number of factors  $k = 5$ , with parameters (reported below) obtained by fitting the skew-t copula with  $\nu = 10$  to  $n = 1040$  observations of 15 minute returns in the period between 2019-Sep-11 and 2019-Nov-6.

$$\alpha = \begin{bmatrix} 0.872 & -0.066 & 0.369 & -5.555 & -0.324 & -0.313 & 0.270 & 0.147 & -0.216 & 0.367 \\ 0.431 & 0.357 & -0.049 & 0.387 & -0.089 & 1.930 & 0.659 & -0.358 & -0.040 & -0.265 \\ 0.326 & 0.346 & -0.450 & 0.271 & -0.786 & 0.070 & -0.098 & -0.447 & -0.004 & -0.414 \end{bmatrix}^\top$$

$$G = \begin{bmatrix} 1831.606 & 0.000 & 0.000 & 0.000 & 0.000 \\ 0.158 & 0.495 & 0.000 & 0.000 & 0.000 \\ 0.198 & 0.411 & 0.013 & 0.000 & 0.000 \\ 0.128 & -0.023 & -0.437 & 0.511 & 0.000 \\ -0.037 & 1.595 & -23.314 & 8.952 & 5.215 \\ 6.425 & -11.706 & -17.094 & 21.695 & -41.596 \\ 0.062 & 0.380 & -0.127 & 0.132 & -0.057 \\ 1.055 & 16.057 & -23.007 & -27.291 & -10.508 \\ 0.119 & 0.188 & -0.263 & 0.138 & -0.203 \\ 0.248 & 0.389 & -0.168 & 0.062 & -0.170 \\ 0.281 & 0.351 & -0.116 & 0.167 & -0.103 \\ 0.151 & 0.161 & -0.293 & 0.232 & -0.512 \\ 6.331 & -11.536 & -16.839 & 21.378 & -40.998 \\ 0.006 & 0.328 & -0.121 & 0.031 & -0.024 \\ 0.029 & 0.555 & -0.431 & -0.165 & -0.186 \\ 0.249 & 0.436 & -0.133 & 0.087 & -0.075 \\ 0.067 & 0.494 & -0.322 & -0.146 & -0.222 \\ 0.114 & 0.459 & -0.149 & 0.087 & -0.199 \\ 0.115 & 0.551 & -0.182 & 0.131 & -0.140 \\ 0.019 & 0.549 & -0.424 & 0.165 & -0.104 \\ 1.050 & 15.973 & -22.878 & -27.142 & -10.458 \\ 0.102 & 0.428 & -0.261 & 0.097 & -0.120 \\ -0.124 & 1.530 & -23.476 & 8.823 & 3.646 \\ 0.005 & 0.507 & -0.284 & -0.045 & -0.136 \\ 82.161 & -0.001 & 0.000 & -0.001 & -0.001 \\ 0.203 & 0.311 & -0.154 & 0.220 & -0.143 \\ 0.203 & 0.445 & -0.214 & 0.122 & -0.155 \\ 0.014 & 0.464 & -0.299 & 0.035 & -0.089 \\ 0.253 & 0.048 & -0.071 & 0.074 & -0.161 \\ 6.351 & -11.576 & -16.895 & 21.442 & -41.113 \end{bmatrix}$$

$$\nu = 10$$

### Part C.2 Additional Empirical Results

Figure A2 plots the marginal posterior means of the four quantile pairwise dependence metrics at the 1% level for Case 1. On the horizontal axis is the exact posterior mean computed using MCMC,

and on the vertical axis is the approximate posterior mean computed using VI. Each point in a scatterplot corresponds to a specific pairwise dependence.

Figure A3 plots the standard deviation of the marginal posterior (i.e. computed using MCMC) and its variational approximation (i.e. computed using VI) for the pairwise Spearman correlations. It is well-known that variational approximations are less well-calibrated to higher order moments, and this is apparent for some of the pairwise Spearman correlations. The accuracy of the variational posterior standard deviations can be further improved by considering more complex variational approximations, although the trade-off typically involves greater computation.

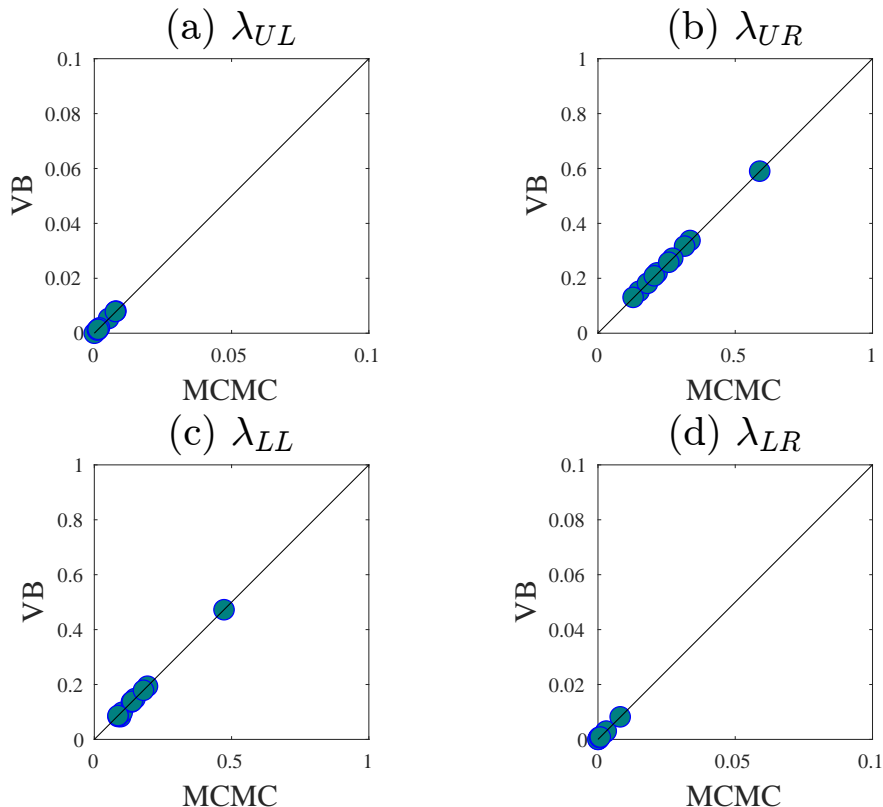


Figure A2: For Case 1, each panel plots the posterior means of the pairwise quantile dependences (at the 1% quantile level). These are computed exactly using MCMC (horizontal axis) and approximately using VI (vertical axis). Each panel gives results for a different direction. The closer the scatters are to the 45 degree line, the more accurate the variational posterior mean.

### Part C.3 Comparison of different generative representations

We find the generative representation GR3 to provide an augmented posterior that is most effective to estimate using our hybrid VI method, in comparison to GR1. To illustrate, Figure A4 plots the logarithm of the posterior density against SGA step for both VI algorithms applied to Case 1. Results are given for the Gaussian factor approximation  $q_\lambda^0$  using  $r = 0, 3$  and 5 factors, and the optimization converges faster by this metric for GR3. Similar results (unreported) were found for Case 2 and in the analysis of the financial data.



Figure A3: The 5-dimensional simulation comparison of the standard deviation of Spearman correlation between MCMC and VB

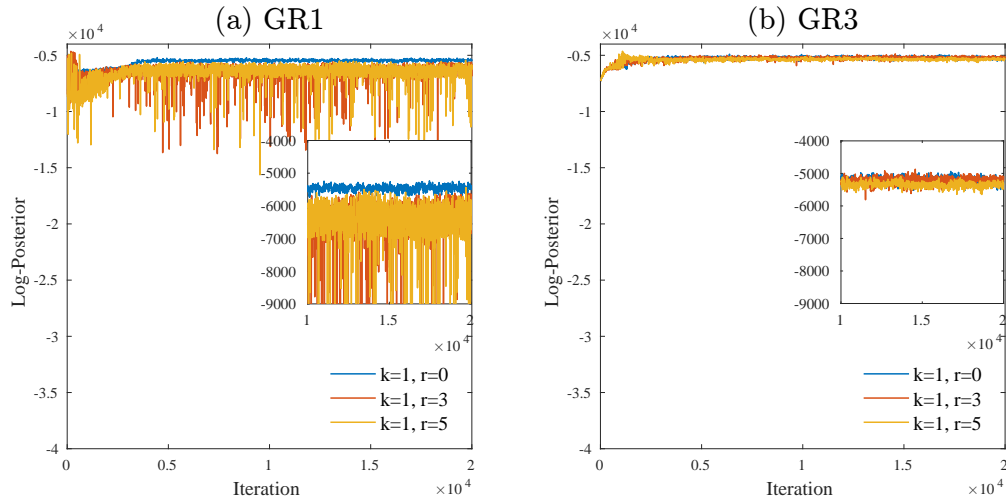


Figure A4: Plots of log-posterior against step number are used to monitor the convergence of the SGA algorithm for the Case 1 simulation. Panel (a) is where generative representation GR1 is used in the hybrid VI algorithm, and panel (b) is where GR3 is used (which is our recommended algorithm).

## Appendix Part D Additional Details for Section 5

### Part D.1 Generating the Predictive Distribution of Portfolio Return

Algorithm 5.1 outlines the steps necessary to generate draws from the posterior predictive return distribution for the density forecast evaluation study in Section 5.3.1.

---

**Algorithm 5.1: Generating from the Predictive Distribution of Portfolio Return**

For  $m = 1, \dots, M$ , do

*Step 1.* Sample skew-t model parameter set  $\theta$  from fitted VB parameters,  $\theta \sim q(\lambda^*)$

*Step 2.* Generate copula data  $\text{vec} \tilde{U} \in \mathbb{R}^d$  from fitted skew-t copula model  $C_{\text{skew-t}}(\text{vec} U = \{U_1, \dots, U_d\}; \theta)$ .

*Step 3.* Transform  $j$ th marginal predicted return from corresponding sampled copula data  $\tilde{z}_{t+1,i}^{(j)} = F_{\text{stud-t}}^{-1}(\tilde{U}_j; \nu_j)$  for  $j = 1, \dots, d$ .

*Step 4.* Then convert it to raw predictive returns  $r_{t+1,i}^{(j)}$ , with GARCH forecasting  $\hat{\sigma}_{t+1,i}$  for  $\tau = 1, \dots, N, j = 1, \dots, d$ , as per the model given in Section 5.1.

$$r_{\tau,t+1}^{(j)} = (h_t s_\tau)^{1/2} \hat{\sigma}_{\tau,t+1} \tilde{z}_{\tau,t+1}^{(j)}$$

*Step 5.* Compute weights  $\omega_j$  from daily shares outstanding  $S_t^{(j)}$  and last price  $P_{\tau,t}^{(j)}$  for each asset.  $K_j = \sum_{t=1}^T S_t^{(j)} P_{\tau,t}^{(j)}$ ,  $\omega_j = K_j / \sum_{j=1}^d K_j$ . These daily market value weighted portfolio compositions are calculated based on data from the Center for Research in Security Prices (CRSP), The University of Chicago Booth School of Business.

*Step 6.* Compute predicted portfolio return

$$R_{\tau,t+1}^{[m]} = \sum_{j=1}^d \omega_j r_{\tau,t+1}^{(j)}$$

.

---

The  $M$  draws of  $(R_{\tau,t+1}^{[1]}, \dots, R_{\tau,t+1}^{[M]})$  represents the draw from the posterior portfolio return distribution. These predictive distributions are evaluated using density forecast evaluation metrics in Section 5.3.1.

### Part D.2 Quantile Dependence of AAPL–MSFT & GOOGL–TSLA

Supplementary results for Section 5.3.2: quantile dependence plots between AAPL – MSFT and GOOGL–TSLA calculated at the peak asymmetry period for each respective pair.

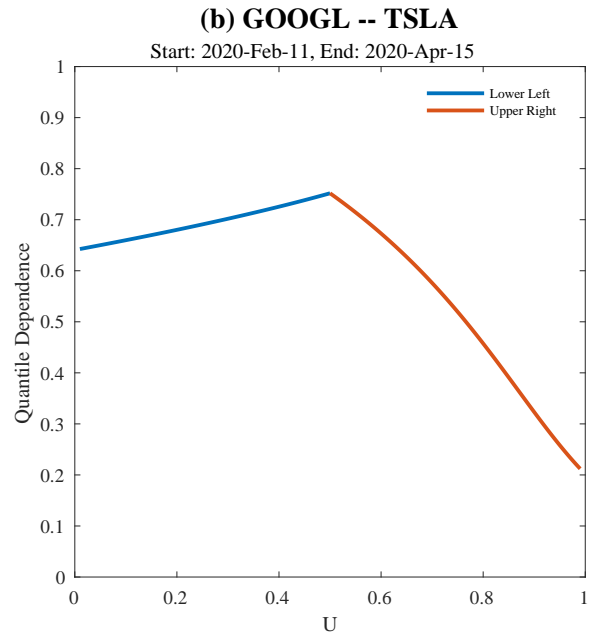
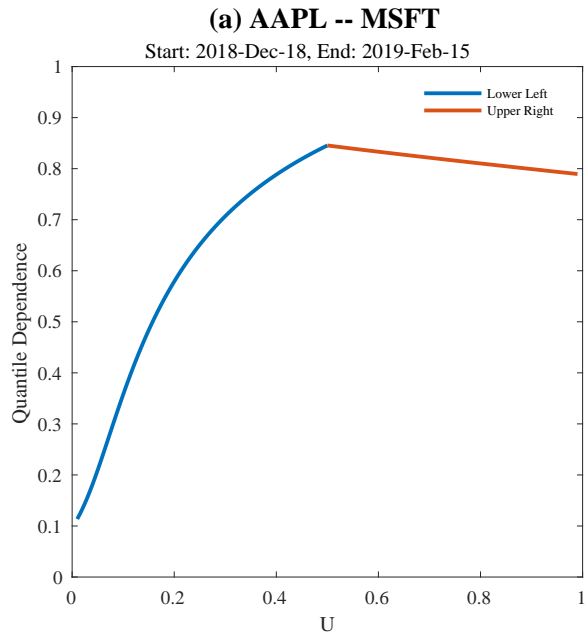


Figure A5: Panel (a) and (b) depict the quantile dependence measure  $\lambda(u)$  along the major diagonals for the peak asymmetry period for Apple vs Microsoft and Google vs Tesla, respectively.